JEM Journal of Experimental Medicine

BRIEF DEFINITIVE REPORT

Altered selection on a single self-ligand promotes susceptibility to organ-specific T cell infiltration

David E.J. Klawon[1*], Dana C. Gilmore[1*], John D. Leonard[2], Christine H. Miller[1], Jaime L. Chao[1], Matthew T. Walker[1], Ryan K. Duncombe[2], Kenneth S. Tung[3], Erin J. Adams[2], and Peter A. Savage[1]

For the large array of self-peptide/MHC class II (pMHC-II) complexes displayed in the body, it is unclear whether CD4⁺ T cell tolerance must be imparted for each individual complex or whether pMHC-II–nonspecific bystander mechanisms are sufficient to confer tolerance by acting broadly on T cells reactive to multiple self-pMHC-II ligands. Here, via reconstitution of T cell–deficient mice, we demonstrate that altered T cell selection on a single prostate-specific self-pMHC-II ligand renders recipient mice susceptible to prostate-specific T cell infiltration. Mechanistically, this self-pMHC-II complex is required for directing antigen-specific cells into the Foxp3⁺ regulatory T cell lineage but does not induce clonal deletion to a measurable extent. Thus, our data demonstrate that polyclonal T reg cells are unable to functionally compensate for a breach in tolerance to a single self-pMHC-II complex in this setting, revealing vulnerabilities in antigen-nonspecific bystander mechanisms of immune tolerance.

Introduction

CD4⁺ T cells recognize short peptides complexed with peptide/MHC class II molecules (pMHC-II) displayed on the surface of APCs. At steady state, antigen processing leads to the presentation of thousands of self-pMHC-II complexes derived from both ubiquitous and tissue-restricted self-proteins. A critical question lies in understanding how the immune system confers T cell tolerance to this vast array of self-pMHC-II ligands while enabling productive T cell responses to pathogen-derived peptides complexed with MHC-II. One model suggests that CD4⁺ T cell tolerance is pMHC-II specific and must be imparted for each self-pMHC-II complex separately. pMHC-II–specific tolerance may be conferred via multiple mechanisms, including deletion or functional inactivation of self-pMHC-II–specific CD4⁺ T conventional (T conv) cells, diversion of such cells into the Foxp3⁺ regulatory T (T reg) cell lineage, and extrinsic pMHC-II–specific suppression of T conv cells by antigen-matched T reg cells. In a competing model, T cell tolerance is conferred in part via pMHC-II–nonspecific mechanisms in which T reg cells engage self-pMHC-II complexes displayed by APCs and suppress the activation of T conv cells reactive to both cognate and unrelated self-pMHC-II ligands. This idea is based on proposed mechanisms of T reg cell–mediated "bystander" suppression, which includes the production of suppressive paracrine factors, depletion of stimulatory factors, or broad dampening of APC stimulatory potential (Josefowicz et al., 2012; Shevach, 2009). The extent to which pMHC-II–specific tolerance and bystander suppression operate in vivo for a single T cell specificity, the specific contexts under which these occur in vivo, and the mechanisms underlying these processes in vivo remain largely undefined.

Seminal studies demonstrated that thymic expression of select tissue-restricted proteins, including the proteins encoded by *Ins2* (Fan et al., 2009) and *Rbp3* (DeVoss et al., 2006), are required for the prevention of spontaneous organ-specific autoimmunity. Given that these proteins each yield multiple antigenic MHC-II–restricted peptides (Taniguchi et al., 2012; Thébault-Baumont et al., 2003), it is not clear whether autoimmunity in these settings is due to a break in T cell tolerance to a single pMHC-II ligand or to multiple pMHC-II specificities acting in concert to promote organ-specific autoimmunity. Here, we examine the role of T cell specificity to pMHC-II in immune tolerance by perturbing the pool of CD4⁺ T cells reactive to a single self-pMHC-II complex and use CD4⁺ T cell transfer to αβ-T cell–deficient mice to define the impact on organ-specific T cell infiltration within a diverse polyclonal T cell repertoire. To do this, we focused on T cell responses to peptides derived from the prostate-specific protein Tcaf3, which is recurrently targeted by autoantibodies and T conv cells in settings of immune

[1]Department of Pathology, University of Chicago, Chicago, IL; [2]Department of Biochemistry and Molecular Biology, University of Chicago, Chicago, IL; [3]Department of Pathology, University of Virginia, Charlottesville, VA.

*D.E.J. Klawon and D.C. Gilmore contributed equally to this paper; Correspondence to Peter A. Savage: psavage@bsd.uchicago.edu.

dysregulation (Malchow et al., 2016; Meng et al., 2011; Setiady et al., 2006). Tcaf3 yields two known I-A^b–restricted self-peptides (termed "C4" and "F1" peptides) that are recognized by naturally occurring T reg cell populations and direct thymic T reg cell differentiation via Aire-dependent processes (Leonard et al., 2017; Malchow et al., 2016). Using mice engineered to express Tcaf3 protein specifically lacking the C4 peptide, we demonstrate that impaired T cell selection on the C4/I-A^b–pMHC-II complex reduces the ratio of C4/I-A^b–specific T reg to T conv cells elicited by immunization and renders T cell–reconstituted mice susceptible to prostate-specific T cell infiltration. Our findings demonstrate that selection on a single self-pMHC-II ligand can be critical for the prevention of organ-specific T cell infiltration, revealing potential vulnerabilities in pMHC-II non-specific bystander mechanisms of tolerance and suggesting that altered T cell selection on a single pMHC-II ligand can predispose to autoimmunity.

Results and discussion

Presentation and recognition of the Tcaf3-derived F1 peptide is unaltered in *Tcaf3(C4)*$^{-/-}$ mice

In this study, we defined how selection on the C4/I-A^b complex impacts the repertoire of antigen-specific T cells in the thymus and periphery and determined the extent to which alterations in this single T cell specificity influence the development of prostatic T cell infiltration in a T cell reconstitution setting. In previous work, we used TCR profiling and T cell stimulation assays to demonstrate that T conv cells reactive to the Tcaf3-derived C4 and F1 peptides recurrently infiltrate the prostates of Aire-deficient mice (Malchow et al., 2016). Consistent with this, we used peptide/MHC tetramer staining here to demonstrate that both C4- and F1-specific T conv cells can be readily detected in the prostates of *Aire*$^{-/-}$ male mice (Fig. S1, A and B). Thus, both C4/I-A^b– and F1/I-A^b–pMHC-II complexes are antigenic and susceptible to spontaneous T cell attack when thymic T cell selection is perturbed via Aire deficiency.

To create a scenario in which T cell selection on a single pMHC-II complex is altered, we used gene-targeted mice in which the germline sequence encoding the 13-aa region of the Tcaf3 protein spanning the C4 peptide is deleted (*Tcaf3(C4)*$^{-/-}$ mice, referred to previously as *Tcaf3*$^{tm1/tm1}$ mice; Leonard et al., 2017). Given that deletion of this 13-aa segment could impact the presentation of the F1 peptide via alterations in Tcaf3 protein expression, stability, or processing, we first set out to determine whether the presentation of the F1 peptide is altered in *Tcaf3(C4)*$^{-/-}$ mice. As expected, primary T conv cells expressing the C4-specific "MJ23" TCR (Malchow et al., 2013) proliferated robustly when cultured with splenic dendritic cells and prostatic lysates from C4-sufficient *Tcaf3(C4)*$^{+/+}$ and *Tcaf3(C4)*$^{+/-}$ mice (collectively denoted as *Tcaf3(C4)*$^{+}$ mice henceforth) but failed to proliferate when extracts from *Tcaf3(C4)*$^{-/-}$ mice were used (Fig. 1, A and B). In contrast, T conv cells expressing the F1-specific "SP33" TCR (Leonard et al., 2017) underwent robust proliferation when cultured with prostatic extracts from mice of all genotypes, indicating that C4 peptide deficiency does not impact the presentation of the F1 peptide in this setting (Fig. 1, A and B). Prostatic extracts from *Tcaf3(C4)*$^{+}$ and *Tcaf3(C4)*$^{-/-}$ mice were also subjected to Western blot analysis using sera from *Aire*$^{-/-}$ mice, which harbor autoantibodies directed against Tcaf3 (Leonard et al., 2017; Setiady et al., 2006). In both cases, blotting identified a protein of the same approximate molecular weight as full-length Tcaf3 in the expected anterior and dorsolateral prostatic lobes (Fig. 1 C; Fujimoto et al., 2006), suggesting that deletion of the 13-aa C4 peptide segment in *Tcaf3(C4)*$^{-/-}$ mice does not impact Tcaf3 protein expression or cause unexpected protein truncation. To analyze presentation of the F1 peptide in vivo, we used naive SP33 T conv cells as a "probe" for antigen recognition. Following transfer of SP33 T conv cells into *Tcaf3(C4)*$^{+}$ or *Tcaf3(C4)*$^{-/-}$ males, we found comparable enrichment and activation of SP33 T cells in the prostate-draining periaortic lymph nodes (Fig. 1, D–F), indicating that F1 peptide presentation is unaltered in vivo in *Tcaf3(C4)*$^{-/-}$ mice.

Selection on C4/I-A^b is required to prevent T cell infiltration of the prostate in a transfer setting

Given that *Tcaf3(C4)*$^{-/-}$ mice lack a single self-peptide, we sought to determine whether T cell selection on the C4/I-A^b complex alone has functional implications for prostate-specific autoimmunity in the absence of additional repertoire changes. *Tcaf3(C4)*$^{-/-}$ mice lack expression of the C4 peptide in the prostate and therefore do not develop prostatic T cell infiltration or hallmarks of prostatitis (data not shown). To create an experimental system in which T cell–dependent prostatitis could be assessed, we performed cell transfer experiments in which 10^7 bulk $CD4^+$ T cells isolated from *Tcaf3(C4)*$^{+}$ or *Tcaf3(C4)*$^{-/-}$ males were transferred into αβ-T cell–deficient *Tcrb*$^{-/-}$*Tcaf3(C4)*$^{+/+}$ male recipients and assessed the impact on T cell infiltration of the prostate 9 wk after transfer. In this way, $CD4^+$ T cells that developed in the presence or absence of the C4 peptide (from *Tcaf3(C4)*$^{+}$ or *Tcaf3(C4)*$^{-/-}$ donor males, respectively) were engrafted into male mice that express the C4 peptide in the prostate. Strikingly, our data revealed that in most recipient mice, the transfer of donor $CD4^+$ T cells from *Tcaf3(C4)*$^{-/-}$ males resulted in prostatic infiltration by C4/I-A^b–specific T cells and polyclonal $CD4^+$ T cells (Fig. 2, A–D). In stark contrast, transfer of $CD4^+$ T cells from *Tcaf3(C4)*$^{+}$ males induced negligible T cell infiltration of the prostate (Fig. 2, A–D). Importantly, C4/I-A^b tetramer$^+$ cells were readily isolated from control cohorts of *Tcrb*$^{-/-}$ recipients that received $CD4^+$ T cells from *Tcaf3(C4)*$^{+}$ donors and were subsequently immunized with the C4 peptide plus complete Freund's adjuvant (CFA), demonstrating that C4/I-A^b–specific T cells exist in the peripheral repertoire of *Tcaf3(C4)*$^{+}$ donor mice and repopulate the peripheral repertoire of recipient mice following T cell transfer (Fig. S1 C). For recipient mice that received T cells from *Tcaf3(C4)*$^{-/-}$ donors, C4/I-A^b tetramer$^+$ T cells in the prostate were largely $Foxp3^-$ (Fig. 2, A and E), whereas $Foxp3^+$ T reg cells accounted for ∼23% of polyclonal C4/I-A^b tetramer$^-$ $CD4^+$ T cells at this site (Fig. 2 F). Consistent with these observations, histological analysis demonstrated that some mice receiving T cells from *Tcaf3(C4)*$^{-/-}$ donors developed mild or severe experimental autoimmune prostatitis (Samy et al., 2005) characterized by overt hallmarks of disrupted tissue architecture and massive infiltration

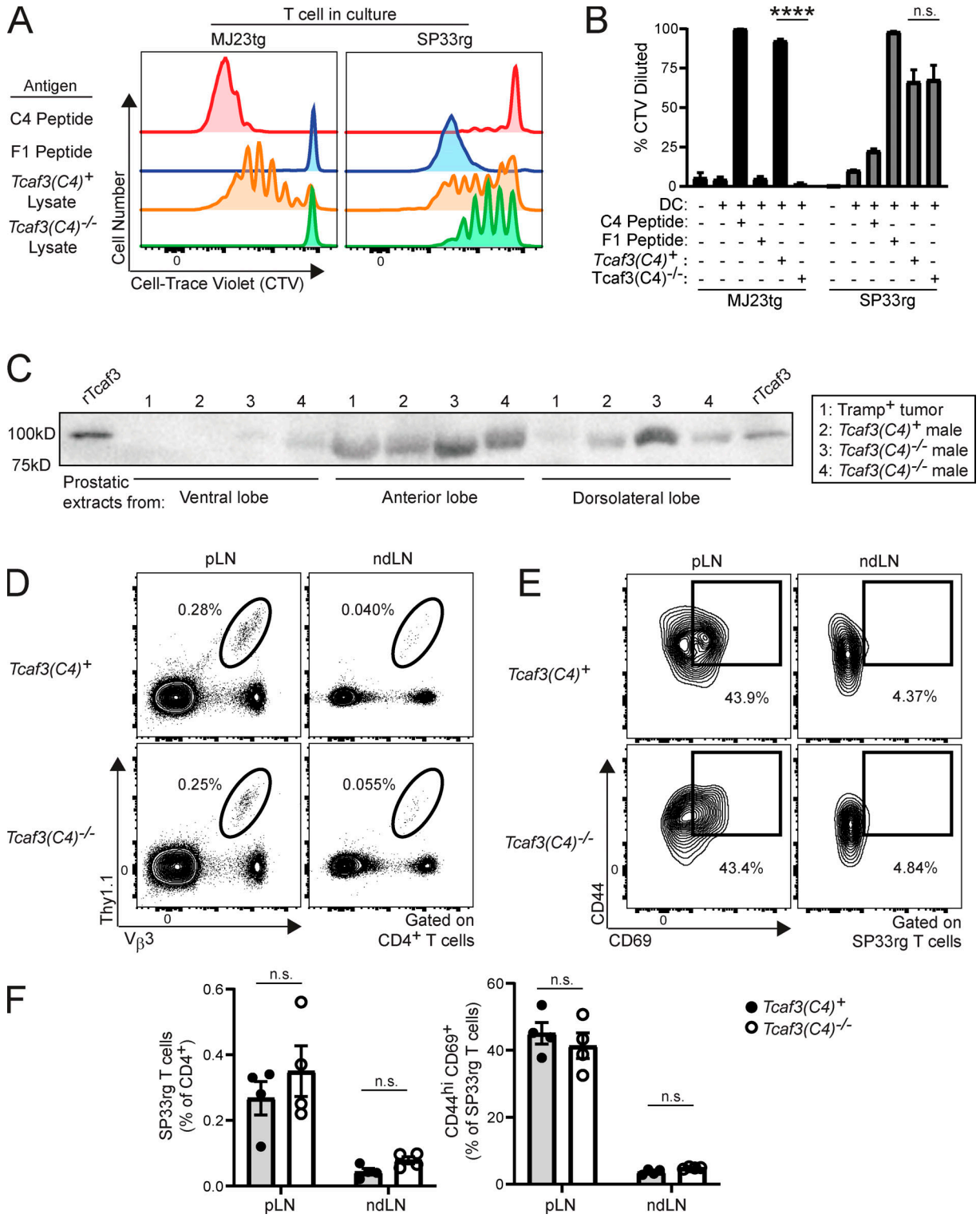

Figure 1. **Presentation and recognition of the Tcaf3-derived F1 peptide are unaltered in *Tcaf3(C4)*$^{-/-}$ mice. (A and B)** In vitro stimulation of MJ23tg or SP33rg T conv cells by prostatic lysates. CD4$^+$ T cells were purified from MJ23tg$^+$ *Rag1*$^{-/-}$ CD45$^{.1/.1}$ transgenic mice (MJ23tg, C4/I-A^b specific) or SP33rg$^+$ Thy1.1$^+$ retrogenic mice (SP33rg, F1/I-A^b specific, see Materials and methods) and labeled with CTV. 10,000 T cells were cocultured with 5 × 10^4 CD11c$^+$ cells isolated from B6 spleens plus rmIL-2, with the indicated purified peptide or prostatic lysates prepared from *Tcaf3(C4)*$^+$ or *Tcaf3(C4)*$^{-/-}$ male littermate mice. Dilution of CTV was assessed by flow cytometry on day 5. **(A)** Representative flow cytometric analysis of CTV dilution by CD4$^+$ MJ23tg or SP33rg T cells. Data are representative of two independent experiments. **(B)** Summary plot of pooled data showing the frequency of MJ23tg or SP33rg cells that have diluted CTV from the indicated cocultures in A. Each sample represents an individual coculture. Mean ± SEM is indicated. *n* = 2, T cell only; *n* = 2, dendritic cell (DC); *n* = 3, C4; *n* = 3, F1; *n* = 3, *Tcaf3(C4)*$^+$; *n* = 3, *Tcaf3(C4)*$^{-/-}$. For both T cell clones, the frequency of divided cells (CTV diluted) following coculture with *Tcaf3(C4)*$^+$ lysate was compared with the frequency of divided cells following coculture with *Tcaf3(C4)*$^{-/-}$ lysate. SP33rg + lysate proliferation index: *Tcaf3(C4)*$^+$, 1.600 ± 0.118;

Tcaf3(C4)$^{-/-}$, 1.520 ± 0.159. ****, P < 0.0001; n.s., P > 0.05; two-tailed Student *t* test. Data are pooled from two independent experiments. **(C)** Prostatic lysates prepared from the prostatic lobes of a tumor-bearing TRAMP^{+} male, a *Tcaf3(C4)*$^{+}$ male, and two *Tcaf3(C4)*$^{-/-}$ males were resolved by SDS-PAGE and subjected to Western blotting with serum from *Aire*$^{-/-}$ mice, which contains Tcaf3-specific autoantibodies. Recombinant Tcaf3 (rTcaf3) was used as a positive control. One representative blot of three independent blots is shown. **(D–F)** In vivo activation and enrichment of F1-specific SP33rg T conv cells in *Tcaf3(C4)*$^{+}$ and *Tcaf3(C4)*$^{-/-}$ males. 10^5 purified SP33rg T cells were transferred intravenously into congenically disparate *Tcaf3(C4)*$^{+}$ or *Tcaf3(C4)*$^{-/-}$ male littermate hosts. 7 d after transfer, cells were isolated from the prostate-draining lymph node (pLN) and nondraining inguinal lymph node (ndLN) and analyzed by flow cytometry. **(D)** Representative flow cytometric analysis of Thy1.1^{+} and $V_\beta3^{+}$ SP33rg T cells among polyclonal CD4^{+} T cells isolated from the indicated lymph node sites in the indicated host mice. The frequency of cells within the indicated gates is denoted. Data are representative of two independent experiments. **(E)** Representative flow cytometric analysis of CD44 vs. CD69 expression by CD4^{+} $V_\beta3^{+}$ SP33rg T cells isolated from the indicated lymph node sites in the indicated host mice. The frequency of cells within the indicated gates is denoted. Data are representative of two independent experiments. **(F)** Left: Summary plot of pooled data from D showing the frequency of CD4^{+} $V_\beta3^{+}$ SP33rg T cells among polyclonal CD4^{+} T cells isolated from the indicated lymph node sites in the indicated host mice. Right: Summary plot of pooled data from E showing the frequency of CD44^{hi} CD69^{+} SP33rg T cells among all CD4^{+} $V_\beta3^{+}$ SP33rg T cells isolated from the indicated lymph node sites in the indicated host mice. Each symbol represents one mouse. *n* = 4, *Tcaf3(C4)*$^{+}$; *n* = 4, *Tcaf3(C4)*$^{-/-}$. Mean ± SEM is indicated (n.s, P > 0.05; two-tailed nonparametric Mann-Whitney test). Data are pooled from two independent experiments.

of CD3^{+} T cells within prostatic glandular structures (Fig. S1 D). Notably, F1/I-A^b tetramer^{+} T cells were rare or not detected in the prostates of recipients reconstituted with T cells from *Tcaf3(C4)*$^{-/-}$ donors (Fig. 2, G–I), demonstrating that the breach in tolerance to C4 peptide did not extend to the Tcaf3-derived F1 peptide. These collective findings demonstrate that in this cell transfer setting, T cell selection on a single self-pMHC-II complex, C4/I-A^b, during formation of the T cell repertoire is required to prevent prostatic T cell infiltration by C4-specific T conv cells and additional polyclonal CD4^{+} T cells of undefined specificity. Importantly, other T reg cell specificities in the donor cell repertoire, including those reactive to the F1 peptide, were unable to functionally compensate for alterations in the pool of C4-specific T cells, suggesting that pMHC-II–nonspecific bystander mechanisms of T reg cell suppression were unable to prevent autoimmune attack by C4-specific T conv cells in this setting.

In the thymus, C4/I-A^b–dependent clonal deletion does not impact the frequency of monoclonal MJ23tg thymocytes

Given the critical nature of T cell selection on the C4/I-A^b complex, we set out to define how selection on C4/I-A^b impacts the thymic development and peripheral pool of C4-specific T cells. The repertoire of these antigen-specific T cells could be shaped by numerous factors, including clonal deletion in the thymus or periphery, differential expansion or survival of T reg cells and T conv cells in the periphery, induction of anergy in C4-specific T conv cells, and differentiation of peripherally induced T reg (pT reg) cells. In previous work, we demonstrated that the thymic development of monoclonal MJ23tg T reg cells requires Aire (Malchow et al., 2013) and depends on expression of the C4 peptide (Leonard et al., 2017). Because Aire has been proposed to promote both clonal deletion and T reg cell generation (Klein et al., 2019), we sought to determine whether thymic presentation of the C4 peptide drives one or both of these alternate cell fates. First, we analyzed thymic development of monoclonal MJ23tg T cells in *Tcaf3(C4)*$^{+}$ and *Tcaf3(C4)*$^{-/-}$ mice following introduction of MJ23tg precursors at low clonal frequencies, a setting required for T reg development due to limited antigenic niches (Bautista et al., 2009; Leung et al., 2009). In one approach, bulk thymocytes from female MJ23tg *Rag1*$^{-/-}$ CD45$^{.1/.1}$ mice, which lack Foxp3^{+} cells due to niche overload (Malchow et al., 2013), were intrathymically injected into *Tcaf3(C4)*$^{+}$ or *Tcaf3(C4)*$^{-/-}$ CD45$^{.2/.2}$ hosts, and donor cells were analyzed 7 d later for expression of Foxp3 and hallmarks of clonal deletion (Fig. 3). In a complementary approach, we generated low-frequency MJ23tg bone marrow chimeras (BMCs) by engrafting bone marrow from MJ23tg *Rag1*$^{-/-}$ CD45$^{.1/.1}$ mice into sublethally irradiated 4–6-wk-old *Tcaf3(C4)*$^{+}$ or *Tcaf3(C4)*$^{-/-}$ CD45$^{.2/.2}$ hosts and analyzed MJ23tg thymocytes 6–8 wk after reconstitution (Fig. S2). The data obtained from these two approaches yielded similar results. As previously shown (Leonard et al., 2017), a fraction of MJ23tg cells developed into Foxp3^{+} T reg cells in the thymus of Tcaf3-sufficient *Tcaf3(C4)*$^{+}$ hosts but not in *Tcaf3(C4)*$^{-/-}$ hosts (Fig. 3, A and B). Consistent with this, a larger fraction of MJ23tg CD4 single-positive (CD4 SP) thymocytes stained positive for PD-1 and CD69 in *Tcaf3(C4)*$^{+}$ hosts relative to *Tcaf3(C4)*$^{-/-}$ hosts, indicative of elevated TCR signaling in response to C4/I-A^b recognition (Fig. 3, C and D). Despite this heightened TCR signaling, we observed no differences in cleaved Caspase-3 staining for MJ23tg thymocytes in *Tcaf3(C4)*$^{+}$ and *Tcaf3(C4)*$^{-/-}$ mice (Fig. 3, A and E), suggesting that recognition of C4/I-A^b does not promote apoptosis to a measurable extent.

Analysis of cleaved Caspase-3 staining alone is insufficient to define the extent of clonal deletion, as the rapid clearance of apoptotic cells in the thymus makes ex vivo identification of such cells challenging, including in carefully controlled model antigen systems (Breed et al., 2019). Therefore, we analyzed clonal deletion using multiple parameters considered together. In the experiments above, we observed no downregulation of the CD4 and CD8 coreceptors (Fig. 3, A, F, and G), an established hallmark of negative selection (Hogquist, 2001). Furthermore, we quantified the fraction of MJ23tg thymocytes making the transition from the CD4^{+}CD8^{+} double-positive (DP) stage to the CD4 SP stage of thymic development (Lee et al., 2012). This transition reflects the entry of maturing thymocytes into the medulla, where Aire is expressed and C4/I-A^b is available for recognition, as evidenced by the specific upregulation of CD69 and PD-1 by CD4 SP but not DP MJ23tg thymocytes (Fig. 3 A). To do this, for each recipient mouse, we plotted the prevalence of MJ23tg cells as the percentage of all DP thymocytes (before C4/I-A^b recognition) vs. the percentage of MJ23tg cells among CD4 SP thymocytes (after or concurrent with C4/I-A^b recognition). If MJ23tg T cells are impacted by clonal deletion following recognition of C4/I-A^b, the relative frequency of MJ23tg thymocytes at the CD4 SP stage is expected to be lower in *Tcaf3(C4)*$^{+}$ hosts

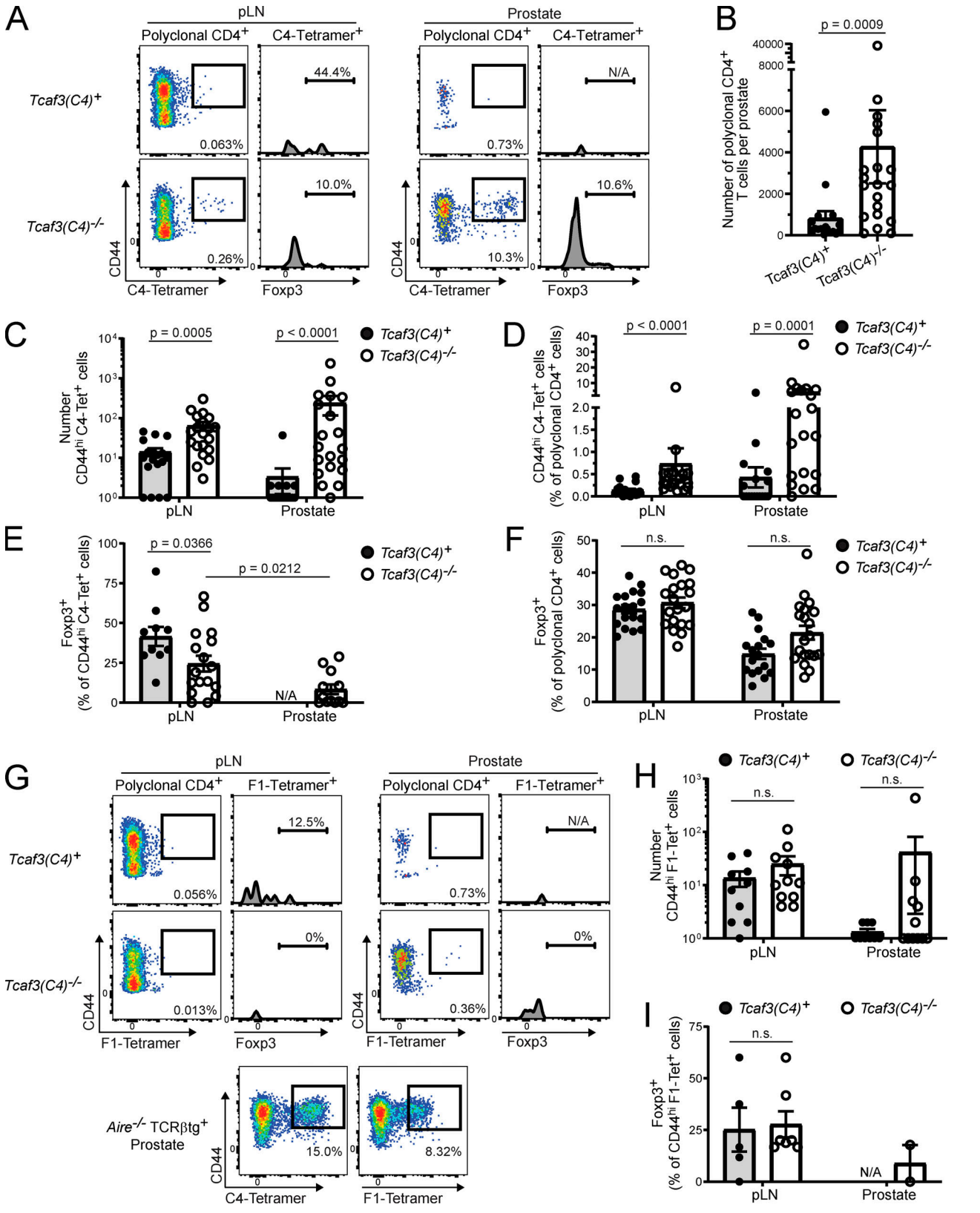

Figure 2. **In a T cell reconstitution setting, T cell selection on C4/I-A^b is required to prevent T cell infiltration of the prostate.** 10^7 polyclonal CD4$^+$ T cells were isolated from the pooled SLOs of 8–12-wk-old *Tcaf3(C4)*$^+$ or *Tcaf3(C4)*$^{-/-}$ male donors and transferred intravenously into *Tcrb*$^{-/-}$ *Tcaf3(C4)*$^{+/+}$ male littermate recipients. 9 wk after transfer, the fate of transferred T cells was assessed in the prostate-draining lymph nodes (pLNs) or prostate. **(A)** Representative flow cytometric analysis of CD4$^+$ T cells isolated from the indicated *Tcrb*$^{-/-}$ host males of the indicated genotype. The left plots depict CD44 vs. C4/I-A^b tetramer$^-$ PE expression by polyclonal CD4$^+$ cells, whereas the right histograms depict Foxp3 expression by CD44^{hi} C4/I-A^b tetramer$^+$ CD4$^+$ T cells. The

frequency of cells within the indicated gates is denoted. Data are representative of six independent experiments. **(B)** Summary plot of pooled data showing the absolute number of polyclonal CD4+ cells isolated from the prostates of host mice. Each symbol represents one mouse. *n* = 18, *Tcaf3(C4)*+ pLN; *n* = 17, *Tcaf3(C4)*+ prostate; *n* = 20, *Tcaf3(C4)*−/−. Mean ± SEM is indicated (two-tailed nonparametric Mann-Whitney test). Data are pooled from six independent experiments. **(C)** Summary plot of the pooled data showing the absolute number of CD44hi C4/I-Ab tetramer+ CD4+ cells isolated from the indicated organs of host mice. Each symbol represents one mouse. *n* = 18, *Tcaf3(C4)*+ pLN; *n* = 17, *Tcaf3(C4)*+ prostate; *n* = 20, *Tcaf3(C4)*−/−. Mean ± SEM is indicated (two-tailed nonparametric Mann-Whitney test). Data are pooled from six independent experiments. **(D)** Summary plot of the pooled data showing the frequency of CD44hi C4/I-Ab tetramer+ CD4+ cells among polyclonal CD4+ T cells isolated from the indicated organs of host mice. Each symbol represents one mouse. *n* = 18, *Tcaf3(C4)*+ pLN; *n* = 17, *Tcaf3(C4)*+ prostate; *n* = 20, *Tcaf3(C4)*−/−. Mean ± SEM is indicated (two-tailed nonparametric Mann-Whitney test). Data are pooled from six independent experiments. **(E)** Summary plot of the pooled data showing the frequency of CD44hi C4/I-Ab tetramer+ CD4+ cells expressing Foxp3 isolated from the indicated organs of host mice. Each symbol represents one mouse. *n* = 10, *Tcaf3(C4)*+ pLN; *n* = 17, *Tcaf3(C4)*−/− pLN; *n* = 12, *Tcaf3(C4)*−/− prostate. Mean ± SEM is indicated (two-tailed nonparametric Mann-Whitney test). Data are pooled from six independent experiments. **(F)** Summary plot of the pooled data showing the frequency of polyclonal CD4+ T cells expressing Foxp3 isolated from the indicated organs of host mice. Each symbol represents one mouse. *n* = 18, *Tcaf3(C4)*+ pLN; *n* = 17, *Tcaf3(C4)*+ prostate; *n* = 20, *Tcaf3(C4)*−/−. Mean ± SEM is indicated (n.s., P > 0.05; two-tailed nonparametric Mann-Whitney test). Data are pooled from six independent experiments. **(G)** Top: Representative flow cytometric analysis of F1/I-Ab tetramer+ CD4+ T cells isolated from the indicated organs of *Tcrb*−/− host males of the indicated genotype. For each site (pLN or prostate), the left plots depict CD44 vs. F1/I-Ab tetramer-allophycocyanin expression by polyclonal CD4+ T cells, whereas the right histograms depict Foxp3 expression by CD44hi F1/I-Ab tetramer+ CD4+ T cells. Bottom: C4/I-Ab and F1/I-Ab tetramer staining positive controls. Representative flow cytometric analysis of CD4+ T cells isolated from the prostate of an *Aire*−/− male expressing a fixed TCRβ transgene (Malchow et al., 2013). The left plot depicts CD44 vs. C4/I-Ab tetramer-PE expression by polyclonal CD4+ T cells, whereas the right plot depicts CD44 vs. F1/I-Ab tetramer-allophycocyanin expression by polyclonal CD4+ T cells. The frequency of cells within the indicated gates is denoted. Data are representative of three independent experiments. **(H)** Summary plot of the pooled data from G showing the absolute number of CD44hi F1/I-Ab tetramer+ CD4+ cells isolated from the indicated organs of host mice. Each symbol represents one mouse. *n* = 10, *Tcaf3(C4)*+ pLN; *n* = 9, *Tcaf3(C4)*+ prostate; *n* = 11, *Tcaf3(C4)*−/−. Mean ± SEM is indicated (n.s., P > 0.05; two-tailed nonparametric Mann-Whitney test). Data are pooled from three independent experiments. **(I)** Summary plot of the pooled data from G showing the frequency of CD44hi F1/I-Ab tetramer+ CD4+ cells expressing Foxp3 isolated from the indicated organs of host mice. Each symbol represents one mouse. *n* = 5, *Tcaf3(C4)*+ pLN; *n* = 7, *Tcaf3(C4)*−/− pLN; *n* = 2, *Tcaf3(C4)*−/− prostate. Mean ± SEM is indicated (n.s., P > 0.05; two-tailed nonparametric Mann-Whitney test). Data are pooled from three independent experiments. N/A, not applicable; Tet+, tetramer+.

relative to *Tcaf3(C4)*−/− hosts, which would be reflected as a downward shift of the best-fit line for data from *Tcaf3(C4)*+ hosts, as depicted in Fig. 3 H. However, the *Tcaf3(C4)*+ and *Tcaf3(C4)*−/− scatter plots of MJ23tg frequencies in *Tcaf3(C4)*+ vs. *Tcaf3(C4)*−/− hosts did not segregate, indicating that the presence of C4 peptide does not impact the relative proportions of MJ23tg precursors at the DP vs. CD4 SP stages to a measurable extent (Fig. 3 H). Collectively, our data indicate that the recognition of C4 peptide directs MJ23tg thymocytes into the T reg cell lineage but plays a negligible role in inducing clonal deletion of this monoclonal specificity.

To extend our analysis of monoclonal MJ23 T cells, we defined the extent to which T cell selection on C4/I-Ab impacts the abundance of endogenous polyclonal C4-specific CD4+ T cells in the thymus. To do this, we quantified rare C4-specific T cells from the thymi of 6–8-wk-old *Tcaf3(C4)*+ or *Tcaf3(C4)*−/− males using a previously established tetramer-based enrichment approach (Legoux and Moon, 2012; Malhotra et al., 2016; Moon et al., 2007). Quantification of double C4/I-Ab tetramer+ thymocytes revealed no significant difference in the absolute number of such cells isolated from the thymi of *Tcaf3(C4)*+ and *Tcaf3(C4)*−/− mice (Fig. 4, A–C; mean of 15 ± 6 and 11 ± 3 cells per two pooled thymi, respectively).

Bim deficiency does not impact the C4/I-Ab tetramer staining intensity of polyclonal C4-specific CD4+ T cells

We next performed studies to determine the extent to which clonal deletion impacts the polyclonal peripheral pool of C4-specific CD4+ T cells. To do this, we used mice lacking the proapoptotic protein Bim that exhibit defects in T cell clonal deletion (Bouillet et al., 2002). Given that very low numbers of C4/I-Ab–specific CD4+ T cells could be detected in unmanipulated naive mice (data not shown), we used an established immunization approach in which antigen-specific CD4+ T cells are expanded via immunization with peptide antigen in CFA, which elicits antigen-specific T cells that are reflective of the preimmunization T cell pool (Moon et al., 2007; Nelson et al., 2015).

We generated mixed BMCs in which lethally irradiated wild-type host mice were reconstituted with a 1:1 mixture of T cell–depleted bone marrow from congenically disparate *Bim*+/+ and *Bim*−/− donors. 5–8 wk later, we immunized chimeric mice with C4 peptide plus CFA, and quantified the relative contributions of the *Bim*+/+ and *Bim*−/− compartments to the pool of C4/I-Ab tetramer+ T cells. In immunized BMC mice, we found that C4/I-Ab tetramer+ C4-specific T cells derived from *Bim*−/− bone marrow accounted for a major fraction (71.4 ± 13%) of C4/I-Ab tetramer+ cells (Fig. 4, D and E). However, this percentage was comparable to that of tetramer-negative polyclonal CD4+ T cells derived from *Bim*−/− precursors in the same mice (74.4 ± 7%; Fig. 4, E and F). Likewise, the fraction of CD8β+ T cells and B220+ B cells derived from the *Bim*−/− compartment was also elevated (accounting for 78.3 ± 9% and 88.8 ± 2% of cells, respectively) in chimeric mice (Fig. 4, F and G). These findings raised the possibility that the increased proportions of lymphocytes derived from *Bim*−/− bone marrow could be due in part to preferential engraftment and survival of *Bim*−/− hematopoietic precursors rather than to a lack of Bim-dependent deletion of T cells or B cells, making it challenging to draw conclusions by examining relative ratios of T cells derived from the *Bim*−/− and *Bim*+/+ compartments. For this reason, we focused our analysis on a paired comparison of C4/I-Ab tetramer+ T cells derived from *Bim*−/− and *Bim*+/+ precursors of immunized mice. If high-avidity C4-specific clones undergo clonal deletion, we reasoned that the mean fluorescence intensity (MFI) of C4/I-Ab tetramer staining, a surrogate marker of TCR–pMHC-II avidity (Crawford et al., 1998; Savage et al., 1999), would be greater for C4/I-Ab tetramer+ cells derived from *Bim*−/− precursors. However, this comparison revealed no

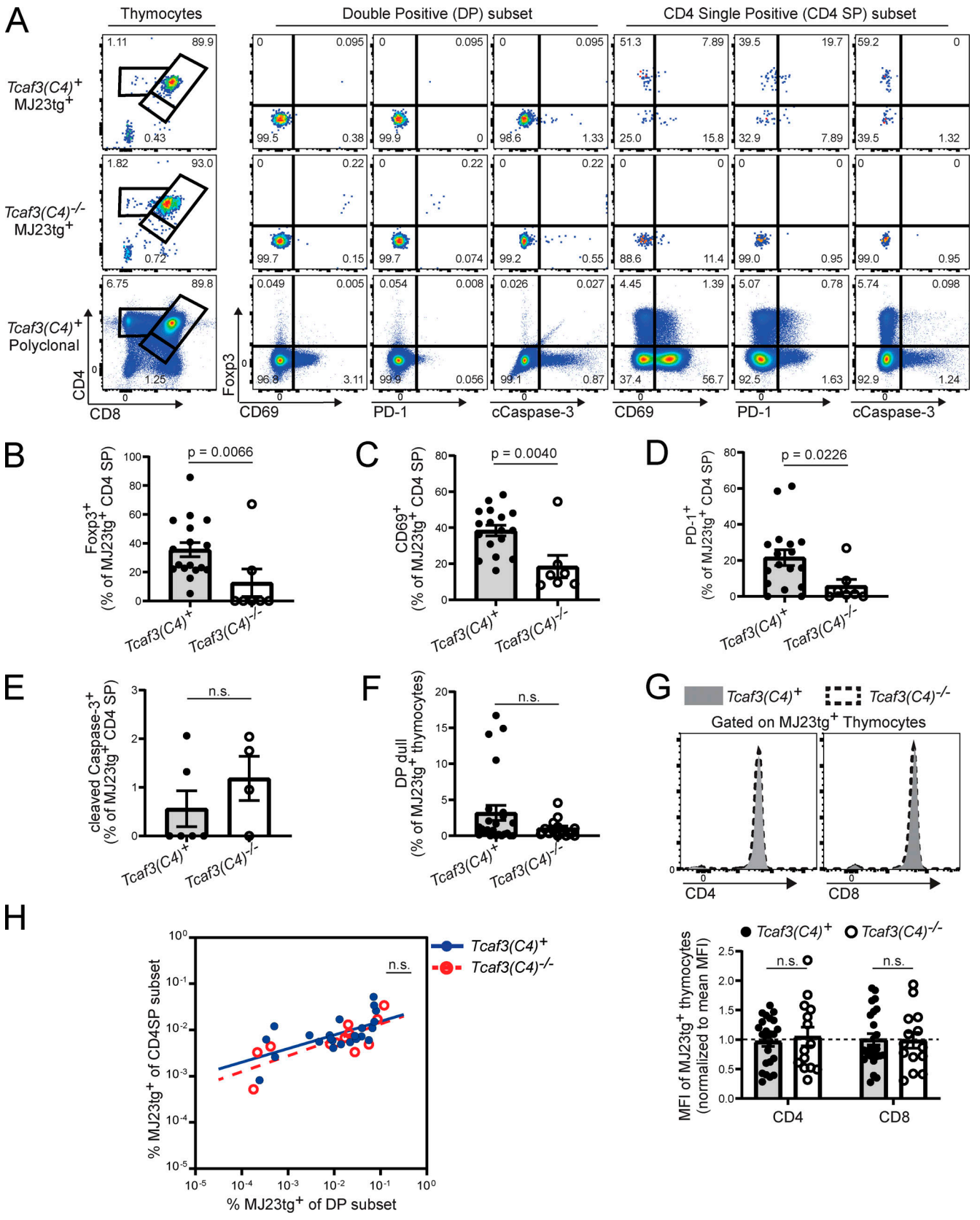

Figure 3. **In the thymus, C4/I-A^b–dependent clonal deletion does not impact monoclonal MJ23tg thymocytes.** Bulk thymocytes from MJ23tg$^+$ *Rag1*$^{-/-}$ CD45$^{.1/.1}$ females, which are uniformly Foxp3$^-$, were transferred intrathymically into 4–6-wk-old male and female *Tcaf3(C4)*$^+$ or *Tcaf3(C4)*$^{-/-}$ littermate hosts and analyzed at day 7 by flow cytometry. **(A)** Representative flow cytometric analysis of MJ23tg (top and middle rows) or polyclonal (bottom row) thymocytes isolated from *Tcaf3(C4)*$^+$ and *Tcaf3(C4)*$^{-/-}$ host mice. The leftmost plots depict CD4 vs. CD8 expression by indicated CD45$^+$ thymocytes, while the remaining

plots depict Foxp3, CD69, PD-1, and cleaved Caspase-3 (cCaspase-3) expression by $CD4^+CD8^+$ DP and CD4 SP thymocytes. The frequency of cells within the indicated gates is denoted. Data are representative of at least two independent experiments. **(B–F)** Summary plots of pooled data from A showing the frequency of MJ23tg CD4 SP thymocytes expressing Foxp3 (B), CD69 (C), PD-1 (D), cCaspase-3 (E), and $CD4^{dull}$ $CD8^{dull}$ (DP dull; F) isolated from the indicated host mice. Each symbol represents one mouse. n = 17, *Tcaf3(C4)*$^+$; n = 7, *Tcaf3(C4)*$^{-/-}$ (B–D). n = 6, *Tcaf3(C4)*$^+$; n = 4, *Tcaf3(C4)*$^{-/-}$ (E). n = 24, *Tcaf3(C4)*$^+$; n = 14, *Tcaf3(C4)*$^{-/-}$ (F). Mean ± SEM is indicated (n.s., $P > 0.05$; two-tailed nonparametric Mann-Whitney test). Data are pooled from multiple independent experiments: four (B–D), two (E), and six (F). **(G)** Top: Representative flow cytometric analysis of CD4 and CD8 expression by MJ23tg thymocytes isolated from the indicated host mice. Bottom: Summary plots of pooled data showing the MFI of CD4 and CD8 by MJ23tg thymocytes isolated from the indicated host mice, normalized to the mean MFI of all MJ23tg thymocytes in each independent experiment. The average MFI of each independent experiment was normalized to 1, indicated by the dashed line. Each symbol represents one mouse. n = 24, *Tcaf3(C4)*$^+$; n = 14, *Tcaf3(C4)*$^{-/-}$. Mean ± SEM is indicated (n.s., $P > 0.05$; two-tailed nonparametric Mann-Whitney test). Data are representative or pooled from six independent experiments. **(H)** Scatter plot depicting the frequency of MJ23tg thymocytes among polyclonal CD4 SP thymocytes vs. the frequency of MJ23tg thymocytes among polyclonal DP thymocytes. Each symbol represents one mouse. n = 24, *Tcaf3(C4)*$^+$; n = 14, *Tcaf3(C4)*$^{-/-}$. Line indicates best-fit curve using linear regression analysis (n.s., $P > 0.05$; extra-sum-of-squares F test). Data are pooled from six independent experiments.

detectable differences in the MFI of tetramer staining between *Bim*$^{-/-}$ and *Bim*$^{+/+}$ C4/I-A^b tetramer$^+$ T cells (Fig. 4 H), suggesting that Bim deficiency does not impact the average avidity of polyclonal C4-specific T cells elicited by peptide immunization. Taken together, our studies of monoclonal and polyclonal populations suggest that C4-dependent clonal deletion has a negligible impact on antigen-specific T cells.

T cell selection on C4/I-A^b promotes T reg skewing of antigen-specific T cells elicited by peptide immunization

Next, we characterized the peripheral pool of C4-specific $CD4^+$ T cells in *Tcaf3(C4)*$^+$ and *Tcaf3(C4)*$^{-/-}$ males using the aforementioned peptide plus CFA immunization approach. *Tcaf3(C4)*$^+$ and *Tcaf3(C4)*$^{-/-}$ mice were immunized, and enriched C4/I-A^b tetramer$^+$ T cells from the pooled secondary lymphoid organs (SLOs) were enumerated and phenotyped 2 wk after immunization (Moon et al., 2009). Our data revealed three notable findings. First, analysis of *Tcaf3(C4)*$^+$ males demonstrated that C4-specific T cells elicited by immunization are skewed to the T reg cell compartment and that skewing is incomplete, averaging 62 ± 14% of Foxp3$^+$ cells in 6–8-wk-old males (Fig. 5, A and B). Second, only 21 ± 13% of C4/I-A^b tetramer$^+$ cells elicited by immunization in *Tcaf3(C4)*$^{-/-}$ mice expressed Foxp3, demonstrating loss of skewing to the T reg cell lineage in C4-deficient mice. Third, the absolute number and tetramer MFI of C4/I-A^b tetramer$^+$ cells recovered after immunization was comparable between *Tcaf3(C4)*$^+$ and *Tcaf3(C4)*$^{-/-}$ males (Fig. 5, C and D). Together, our cumulative findings indicate that C4/I-A^b–specific T conv cells and T reg cells coexist in the peripheral repertoire of wild-type mice and that C4/I-A^b largely functions to direct antigen-specific T cells to the T reg cell lineage, with negligible evidence of clonal deletion.

Collective evidence from the current and previous studies (Leonard et al., 2017; Malchow et al., 2016; Malchow et al., 2013) demonstrates that C4/I-A^b directs T reg cell differentiation in the thymus. Consistent with this, we found that C4/I-A^b tetramer$^+$ cells elicited by peptide immunization uniformly express high densities of Helios (Fig. S3, A and B), which has been implicated as a potential marker of thymus-derived T reg cells (Thornton et al., 2010). Nonetheless, it remained possible that pT reg cells contribute to the pool of C4/I-A^b tetramer$^+$ cells elicited by immunization with C4 peptide plus CFA. To assess this possibility, *Tcrb*$^{-/-}$ male recipients were reconstituted with 10^6 Foxp3$^+$ cells purified from *Foxp3*^{GFP} reporter mice, together with 7 × 10^6 Foxp3$^-$ cells purified from congenically distinct *Foxp3*^{GFP} mice. 3 wk later, recipient mice were immunized with C4 peptide plus CFA and analyzed at 2 wk after challenge (Fig. S3 C). Of the C4/I-A^b tetramer$^+$ Foxp3$^+$ T reg cells elicited by immunization, nearly all Foxp3$^+$ cells were derived from the preexisting Foxp3$^+$ donor cell population, whereas C4/I-A^b Foxp3$^-$ cells were largely derived from the Foxp3$^-$ donor cell population, indicating that immunization-induced pT reg cells make minimal contributions to the pool of C4-specific T reg cells in this setting (Fig. S3, D and E).

In this study, we use a T cell reconstitution system to demonstrate that altered T cell selection on a single self-pMHC-II complex, C4/I-A^b, renders B6 male mice susceptible to prostate-specific T cell infiltration. This finding indicates that T cell tolerance to the C4/I-A^b self-ligand is pMHC-II specific and implies that polyclonal T reg cells reactive to other pMHC-II ligands, including I-A^b complexed with the Tcaf3-derived F1 peptide, are unable to compensate for alterations in the C4/I-A^b–specific T cell pool. Broadly, our findings reveal that pMHC-II nonspecific bystander mechanisms of T reg–mediated suppression are insufficient to prevent targeted T cell–mediated autoimmunity in this setting and suggest a crucial requirement for pMHC-II–specific T reg suppression. Ultimately, these concepts suggest that vulnerabilities in tolerance to single pMHC-II specificities may predispose individuals to the development of organ-specific autoimmunity and support a model in which the generation of a diverse T reg cell repertoire spanning a broad array of pMHC-II specificities is essential for maintaining T cell tolerance by providing full "coverage" of antigenic pMHC-II complexes throughout the body.

It is important to note that the breach in tolerance observed in our experiments occurred following $CD4^+$ T cell transfer to αβ-T cell–deficient recipients, a setting that may potentiate T cell activation and differentiation due to homeostatic proliferation of donor cells in the lymphopenic host. This environment mirrors the natural setting of lymphopenia and homeostatic proliferation that is well documented in the neonatal period, a time span that is crucial for the establishment of T cell tolerance, especially to Aire-dependent tissue-restricted antigens (Yang et al., 2015). Relatedly, it is possible that the differentiation of C4-specific T reg cells is especially robust in the neonatal period (Yang et al., 2015), which may confer these cells with a superior capacity to prevent organ-specific autoimmunity. It remains unclear whether altered T cell selection on C4/I-A^b is sufficient to

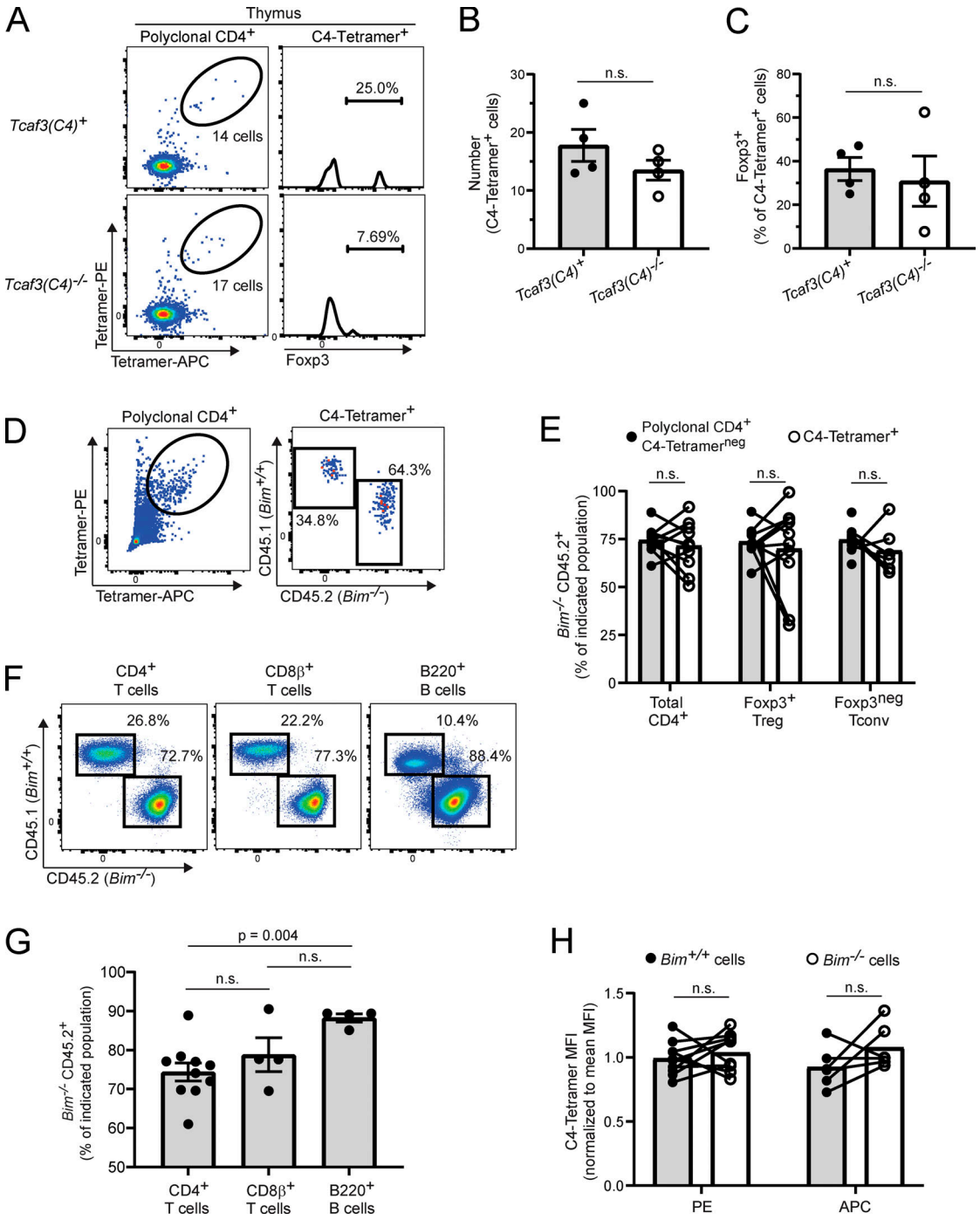

Figure 4. **C4/I-A^b–dependent clonal deletion does not impact the endogenous pool of C4/I-A^b–specific polyclonal CD4$^+$ T cells. (A–C)** C4/I-A^b tetramer analysis of polyclonal thymocytes from *Tcaf3(C4)*$^+$ or *Tcaf3(C4)*$^{-/-}$ mice. **(A)** Representative flow cytometric analysis of CD4 SP thymocytes enriched from two pooled thymi from 4–6-wk-old mice of the indicated genotype. The left plots depict dual C4/I-A^b tetramer expression by polyclonal CD4 SP thymocytes, whereas the right plots depict Foxp3 expression by double C4/I-A^b tetramer$^+$ CD4 SP thymocytes. The absolute number of cells (left) and frequency of cells (right) within the indicated gates are denoted. Data are representative of four independent experiments. **(B)** Summary plot of pooled data from A showing the absolute number of double C4/I-A^b tetramer$^+$ thymocytes enriched from two pooled thymi from mice of the indicated genotype. Each symbol represents cells pooled from two mice. n = 4, *Tcaf3(C4)*$^+$; n = 4, *Tcaf3(C4)*$^{-/-}$. Mean ± SEM is indicated (n.s., P > 0.05; two-tailed nonparametric Mann-Whitney test). Data are pooled from four independent experiments. **(C)** Summary plot of pooled data from A showing the frequency of double C4/I-A^b tetramer$^+$ CD4 SP thymocytes expressing Foxp3 enriched from two pooled thymi from mice of the indicated genotype. Each symbol represents cells pooled from two mice. n = 4, *Tcaf3(C4)*$^+$; n = 4, *Tcaf3(C4)*$^{-/-}$. Mean ± SEM is indicated (n.s., P > 0.05; two-tailed nonparametric Mann-Whitney test). Data are pooled from four independent experiments. **(D–H)** Analysis of C4/I-A^b tetramer$^+$ T cells elicited by immunization in *Bim*$^{+/+}$/*Bim*$^{-/-}$ mixed BMC mice. 6–8-wk-old B6.SJL (CD45$^{.1/.1}$) male littermate mice were lethally irradiated and reconstituted with a 1:1 mixture of *Bim*$^{+/+}$ (CD45.1) and *Bim*$^{-/-}$ (CD45.2) bone marrow. 5–8 wk after engraftment, mice were immunized subcutaneously with 100 µg of C4 peptide emulsified in CFA. 14 d after immunization, CD4$^+$ T cells were isolated, and C4/I-A^b tetramer-binding cells were enriched from the pooled SLOs and analyzed by flow cytometry. **(D)** Representative flow cytometric analysis of CD4$^+$ T cells enriched from the

pooled SLOs of immunized mixed BMC mice. The left plot depicts dual C4/I-A^b tetramer expression by polyclonal CD4$^+$ T cells, whereas the right plot depicts CD45.2 vs. CD45.1 expression by C4/I-A^b tetramer$^+$ CD4$^+$ T cells. The frequency of cells within the indicated gates is denoted. Data are representative of two independent experiments. **(E)** Summary plot of data pooled from D showing the frequency of C4/I-A^b tetramer$^-$ and C4/I-A^b tetramer$^+$ CD4$^+$ T cells expressing CD45.2 enriched from the SLOs of immunized mixed BMC mice. Each symbol represents one mouse (n = 10). Mean ± SEM is indicated (n.s., P > 0.05; Wilcoxon matched-pairs signed rank test). Data are pooled from two independent experiments. **(F)** Representative flow cytometric analysis of CD45.2 vs. CD45.1 expression by bulk CD4$^+$, CD8β$^+$, and B220$^+$ cells isolated from the SLOs of immunized mixed BMC mice. The frequency of cells within the indicated gates is denoted. Data are representative of two independent experiments. **(G)** Summary plot of data pooled from F showing the percentage of CD45.2$^+$ cells among all CD4$^+$, CD8β$^+$, and B220$^+$ cells isolated from the SLOs of immunized chimeric mice; CD45.2 denotes cells derived from *Bim*$^{-/-}$ bone marrow. Each symbol represents data from one mouse. n = 10, CD4; n = 4, CD8β; n = 4, B220. Mean ± SEM is indicated (n.s., P > 0.05; two-tailed nonparametric Mann-Whitney test). Data are pooled from two independent experiments. **(H)** Summary plots of pooled data from D showing the MFI of C4/I-A^b tetramer-PE and C4/I-A^b tetramer-allophycocyanin (APC) by C4/I-A^b tetramer$^+$ CD4$^+$ CD45.2$^+$ and C4/I-A^b tetramer$^+$ CD4$^+$ CD45.1$^+$ cells enriched from the SLOs of immunized mixed BMC mice, normalized to the mean MFI of all C4/I-A^b tetramer$^+$ CD4$^+$ cells in each independent experiment. Each symbol represents one mouse. n = 10, PE; n = 6, APC. Mean ± SEM is indicated (n.s., P > 0.05; Wilcoxon matched-pairs signed rank test). Data are pooled from two independent experiments.

induce prostatic T cell infiltration in a lymphoreplete adult host in the absence of innate immune activation or homeostatic proliferation. Of note, our current findings using T cell transfer are consistent with our prior studies in unmanipulated *Aire*$^{-/-}$ mice (Leonard et al., 2017; Malchow et al., 2016), which demonstrated that both C4/I-A^b and F1/I-A^b are spontaneously targeted by prostate-infiltrating T conv cells in settings of Aire deficiency.

Mechanistically, our data from multiple complementary approaches indicate that C4/I-A^b–dependent clonal deletion has a negligible impact on polyclonal and monoclonal C4/I-A^b–specific T cells. Instead, our data support the premise that T reg cell differentiation is the primary fate of developing thymocytes reactive to the C4/I-A^b complex. This finding is consistent with a recent study of polyclonal CD4$^+$ T cells reactive to peptide epitopes derived from proteolipid protein (PLP), which demonstrated that thymic expression of PLP does not lead to the loss of PLP-specific T cell clonotypes in the thymus but, instead, directs a fraction of these clones into the T reg cell lineage (Hassler et al., 2019). In our system, it remains to be determined whether loss of tolerance to C4/I-A^b is due to qualitative or quantitative alterations in C4-specific T reg cells, C4-specific T conv cells, or both.

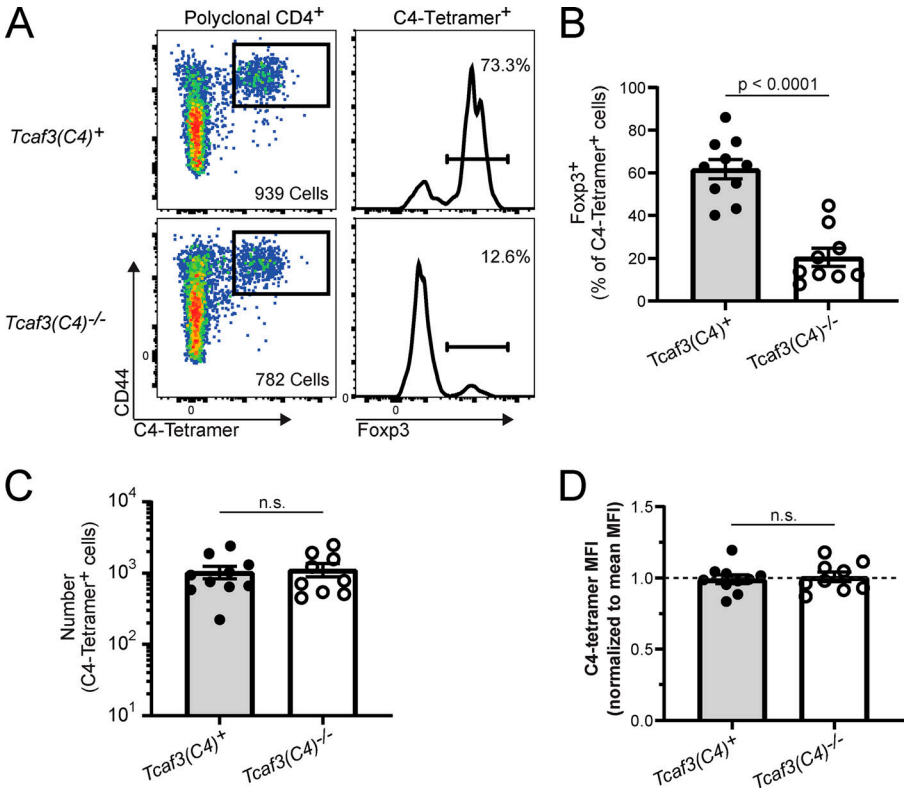

Figure 5. **T cell selection on C4/I-A^b promotes T reg skewing of antigen-specific T cells elicited by C4 peptide immunization.** 4–8-wk-old naive *Tcaf3(C4)*$^+$ or *Tcaf3(C4)*$^{-/-}$ male littermate mice were immunized subcutaneously with 100 µg C4 peptide emulsified in CFA. 14 d after immunization, CD4$^+$ T cells were isolated, and C4/I-A^b tetramer-binding cells were enriched from the pooled SLOs and analyzed by flow cytometry. **(A)** Representative flow cytometric analysis of CD4$^+$ T cells enriched from the pooled SLOs of mice of the indicated genotype. The left plots depict CD44 vs. C4/I-A^b tetramer-PE expression by polyclonal CD4$^+$ T cells, whereas the right plots depict Foxp3 expression by CD44^{hi} C4/I-A^b tetramer$^+$ CD4$^+$ T cells. The absolute number of cells (left) and frequency of cells (right) within the indicated gates are denoted. Data are representative of three independent experiments. **(B)** Summary plot of data pooled from A showing the frequency of CD44^{hi} C4/I-A^b tetramer$^+$ CD4$^+$ cells expressing Foxp3 enriched from the pooled SLOs from mice of the indicated genotype. Each symbol represents one mouse. n = 10, *Tcaf3(C4)*$^+$; n = 9, *Tcaf3(C4)*$^{-/-}$. Mean ± SEM is indicated (two-tailed nonparametric Mann-Whitney test). Data are pooled from three independent experiments. **(C)** Summary plot of pooled data from A showing the absolute number of CD44^{hi} C4/I-A^b tetramer$^+$ CD4$^+$ cells enriched from the pooled SLOs from mice of the indicated genotype. Each symbol represents one mouse. n = 10, *Tcaf3(C4)*$^+$; n = 9, *Tcaf3(C4)*$^{-/-}$. Mean ± SEM is indicated (n.s., P > 0.05; two-tailed nonparametric Mann-Whitney test). Data are pooled from three independent experiments. **(D)** Summary plots of pooled data from A showing the MFI of C4/I-A^b tetramer-PE for CD44^{hi} C4/I-A^b tetramer$^+$ CD4$^+$ cells enriched from mice of the indicated genotype, normalized to the mean MFI of all CD44^{hi} C4/I-A^b tetramer$^+$ CD4$^+$ cells in each independent experiment. The average MFI of each independent experiment was normalized to 1, indicated by the dashed line. Each symbol represents one mouse. n = 10, *Tcaf3(C4)*$^+$; n = 9, *Tcaf3(C4)*$^{-/-}$. Mean ± SEM is indicated (n.s., P > 0.05; two-tailed nonparametric Mann-Whitney test). Data are pooled from three independent experiments.

Materials and methods

Mice

The following mice were purchased from The Jackson Laboratory and bred and maintained at the University of Chicago: C57BL/6J (B6) mice; CD45.1/.1 B6.SJL-*Ptprc*^{a} *Pepc*^{b}/*BoyJ* mice; TRAMP C57BL/6-Tg(TRAMP)8247Ng/J mice; *Rag1*$^{-/-}$ B6.129S7-*Rag1*^{tm1Mom}/J mice; *Aire*$^{-/-}$ B6.129S2-*Aire*$^{tm1.1Doi}$/J mice; TCRα$^{-/-}$ B6.129S2-*Tcra*^{tm1Mom}/J mice; *Bim*$^{-/-}$ B6.129S1-*Bcl2l11*$^{tm1.1Ast}$/J, *Foxp3*^{GFP} B6.Cg-*Foxp3*^{tm2Tch}/J, CD4-Cre B6.Cg-Tg(Cd4-cre)1Cwi/BfluJ mice; and *Tcrb*$^{-/-}$ B6.129P2-*Tcrb*^{tm1Mom}/J mice. MJ23tg *Rag1*$^{-/-}$ CD45.1/.1 and "TCRβtg" mice expressing a fixed TCRβ chain of sequence TRBV26-ASSLGSSYEQY were generated as described previously (Malchow et al., 2013). *Tcaf3(C4)*$^{-/-}$ mice were generated as described previously, under the alias "*Tcaf3*^{tm1}" (Leonard et al., 2017). All mice were generated on a pure B6 background or were fully backcrossed to the B6 background. All mice were bred and maintained under specific pathogen–free conditions in accordance with the animal care and use regulations of the University of Chicago, Association for Assessment and Accreditation of Laboratory Animal Care Unit #001020, Public Health Service Policy on Humane Care and Use of Laboratory Animals policy assurance #D16-00322 (A3523-01), and United States Department of Agriculture registration #33-R0151. Mice were housed in sterile and ventilated microisolation cages, up to five mice per cage, and fed irradiated standard pellet chow and reverse osmosis water ad libitum in a 12-h light/dark cycle, with room temperature at 22 ± 1°C. All cages contained sterile quarter-inch corncob bedding and a nestlet for environmental enrichment. Mice for experiments were age-matched, littermates when possible, and assigned to experimental groups based on genotype.

Cell lines and bacteria

High Five insect cells (*Trichoplusia ni*, female, ovarian) were used for production of recombinant Tcaf3. Cells were grown in Insect-XPRESS Protein-Free Insect Cell Medium supplemented with additional L-glutamine (2 mM) and gentamicin sulfate (50 µg/ml) in suspension culture and shaken at 120 revolutions per minute at 27°C. *Drosophila* S2 cells were used for recombinant production of I-A^{b}; cells were transfected according to the *Drosophila* Expression System manual (Thermo Fisher Scientific) in Schneider's *Drosophila* Medium supplemented with 10% FBS, 1× pen/strep (100 U/ml penicillin, 0.1 mg/ml streptomycin), and 20 µg/ml gentamicin and maintained in stationary cultures at 27°C. S2 transfectants were selected with 25 µg/ml blasticidin, and stable lines were expanded for expression in Express Five Serum Free Media supplemented with 25 µg/ml blasticidin, 1× pen/strep, and 20 µg/ml gentamicin in suspension culture shaken at 120 revolutions per minute at 27°C. Platinum-E (Plat-E) cells (Cell Biolabs) were used for retroviral packaging of SP33 TCRα-containing pMGflThy1.1 plasmid; cells were grown in DMEM (Gibco) supplemented with 10% FBS, 1× pen/strep, 10 µg/ml blasticidin, and 1 µg/ml puromycin and maintained in stationary cultures at 37°C. Plat-E transfectants were cultured in the absence of blasticidin and puromycin. *Escherichia coli* DH5α (New England Biolabs) was used for cloning and propagation of SP33 TCRα-containing pMGflThy1.1 plasmid.

Retrovirus production, infection, and generation of SP33 retrogenic (SP33rg) mice

SP33rg mice were generated as described previously (Leonard et al., 2017; McDonald et al., 2015). In brief, the SP33 TCRα was cloned into a retroviral construct modified from Turner and colleagues (McDonald et al., 2015; Turner et al., 2010). Plat-E cells, also previously described (Morita et al., 2000), were used to generate retrovirus. *TCRα*$^{-/-}$ CD4-Cre^{+} TCRβtg^{+} mice on a B6 background were injected with 5-fluorouracil (APP Pharmaceuticals) 3 d before bone marrow harvest. Bone marrow cells were cultured for 2 d in X-VIVO 10 (Lonza) containing 15% FCS, 1% pen/strep, 100 ng/ml mouse stem cell factor, 10 ng/ml mouse IL-3, and 20 ng/ml mouse IL-6 (BioLegend). Cells were infected with retrovirus by spinfection in the presence of 6 µg/ml polybrene (EMD Millipore) and cultured for an additional 24 h. All spinfected cells were then mixed with 5 × 10^{6} freshly harvested bone marrow "filler" cells from *Rag1*$^{-/-}$ mice and injected into lethally irradiated (900 rads) CD45.1/.1 *B6.SJL* recipient mice to generate SP33rg mice. SP33rg cells were isolated from retrogenic mice 6–8 wk after bone marrow reconstitution. CD4^{+} T cells were FACS–purified from SP33rg mice following CD4 MACS (Miltenyi Biotec) enrichment and staining with the following antibodies: anti-CD8b (Ly-3), anti-CD45.1 (A20), anti-CD45.2 (104), and anti-Thy1.1 (OX-7).

Preparation of prostatic extracts

The procedure for the preparation of prostatic secretory extracts was adapted from Fujimoto et al. (2006). Prostates of tumor-bearing TRAMP^{+} male mice 6 mo of age or age-matched *Tcaf3(C4)*$^{+}$ or *Tcaf3(C4)*$^{-/-}$ males 6–8 wk of age were dissected to separate the anterior, ventral, and dorsolateral lobes or were left intact, as indicated in the figure legends. The dissected tissues were incubated separately in 1–2 ml PBS for 5 min at room temperature to extract secreted proteins and then spun for 5 min at 10,000 ×*g* at 4°C. The supernatant was transferred to a fresh tube and spun again for 5 min at 13,200 ×*g* at 4°C. The supernatant from this second spin was retained, and total protein content was quantified by BCA Protein Assay Kit (Pierce). These extracts (prostatic lysates) were flash frozen in liquid nitrogen and stored at −80°C until use.

Production of recombinant Tcaf3 protein

Tcaf3 was produced recombinantly in High Five insect cells (Thermo Fisher Scientific) as previously described (Leonard et al., 2017). In brief, the Tcaf3 protein sequence (GenBank accession no. NM_203396.1) was fused at its N-terminus to the gp67 secretion signal sequence, an 8xHis tag, a 3C protease cleavage site, and intervening linker sequences. Tagged protein was purified from culture supernatant by nickel affinity chromatography, and the His tags were removed by cleavage with 3C protease. Protease and uncleaved proteins were removed by a second pass over nickel resin. Purified Tcaf3 was exchanged into PBS using a Zeba Desalting Spin Column (Thermo Fisher Scientific) and sterilized by 0.22-mm filtration.

In vitro T cell stimulation

CD4^{+} T cells were isolated from MJ23tg^{+} *Rag1*$^{-/-}$ CD45.1/.1 female donor mice and purified by MACS (Miltenyi Biotec) enrichment.

$CD4^+$ SP33rg T cells were purified by FACS as described above. $CD4^+$ T cells were labeled with CellTrace Violet (CTV; Thermo Fisher Scientific) per the manufacturer's instructions with slight modification. In brief, cells were pelleted, resuspended in CTV at 1:1,000 dilution, and incubated for 20 min at 37°C. The reaction was quenched by the addition of 13 ml PBS. To isolate splenic dendritic cells, splenocytes were isolated from B6 mice and enriched for $CD11c^+$ cells via MACS-positive selection (Miltenyi Biotec). 10^4 CTV-labeled T cells were cocultured with 5×10^4 $CD11c^+$ splenocytes, 100 U/ml recombinant mouse IL-2 (Miltenyi Biotec), and prostatic extract or peptide as indicated. Cell cultures were set up in 384-well, ultra-low attachment, round-bottom plates (Corning). Dilution of CTV was assessed by flow cytometry on day 5.

Tcaf3 Western blot

Serum was isolated from *Aire*$^{-/-}$ males at varying ages. 100 ng recombinant Tcaf3 protein or 10 µg prostatic lysate were loaded onto a 15-well, 4–20% SDS-PAGE gel (~38 ng protein per mm lane width; Bio-Rad) and transferred to nitrocellulose membrane. The membrane was blocked for 1 h at room temperature with 3% wt/vol BSA in TBSt (20 mM Tris, pH 7.5, 150 mM NaCl, 0.1% vol/vol Tween 20) and then blotted overnight at 4°C with *Aire*$^{-/-}$ sera diluted 1:800 in TBSt + 3% wt/vol BSA + 0.1% wt/vol sodium azide. The membrane was washed with TBSt and blotted for 1 h at room temperature with bovine anti-mouse–IgG HRP conjugate (sc-2371; Santa Cruz Biotechnology) diluted 1:10,000 in TBSt + 5% wt/vol nonfat dried milk. The membrane was washed with TBSt, incubated with SuperSignal West Pico Chemiluminescent Substrate (Thermo Fisher Scientific), and imaged on a ChemiDoc imager (Bio-Rad).

T cell transfer experiments

Polyclonal donor T cells

Cells from pooled spleen and lymph nodes (axillary, brachial, cervical, inguinal, pancreatic, and periaortic) from 8–12-wk-old *Tcaf3(C4)*$^+$ or *Tcaf3(C4)*$^{-/-}$ male mice were enriched for $CD4^+$ T cells by MACS (Miltenyi Biotec) and combined, and 10^7 cells were injected retro-orbitally into 6–10-wk-old *Tcrb*$^{-/-}$ male hosts.

Congenically distinct T reg and T conv cells

Cells from pooled spleen and lymph nodes (axillary, brachial, cervical, inguinal, pancreatic, and periaortic) from 8–12-wk-old *Foxp3*^{GFP} CD45$^{.1./.1}$ or *Foxp3*^{GFP} CD45$^{.2./.2}$ male mice were enriched for $CD4^+$ T cells by MACS (Miltenyi Biotec) and sorted as by FACS as $Foxp3^+$ T reg and $Foxp3^{neg}$ T conv cells. A congenically disparate mixture of 10^6 $Foxp3^+$ and 7×10^6 $Foxp3^-$ cells was injected retro-orbitally into 6–10-wk-old *Tcrb*$^{-/-}$ male hosts, and the fate of donor T conv cells was assessed by flow cytometry at times indicated in the figure legends.

I-A^b tetramer production

C4/I-A^b tetramers bearing the $Tcaf3_{646–658}$(648Y) peptide (THYKAPWGELATD) and F1/I-A^b tetramers bearing the $Tcaf3_{88-107}$ peptide (CPGAPIAVHSSLASLVNILG) were produced using methods similar to those described previously (Moon et al., 2007). I-A^b was expressed in *Drosophila* S2 cells, using separate plasmids to encode the α- and β-chains, as described previously (Moon et al., 2007). Constructs were cotransfected into *Drosophila* S2 cells together with a plasmid encoding the BirA biotin ligase. Protein expression was induced with the addition of 0.8 mM $CuSO_4$ in the presence of 2 µg/ml biotin (Sigma-Aldrich). Biotinylated I-A^b protein was purified from culture supernatant by nickel affinity chromatography with His Bind Ni-IDA Resin (EMD Millipore) and by avidin affinity chromatography with Pierce Monomeric Avidin UltraLink Resin (Thermo Fisher Scientific). Tetramers were formed by mixing biotinylated I-A^b with streptavidin-allophycocyanin (PJ27S; ProZyme) or streptavidin-PE (PJRS34; ProZyme) at a slight molar excess of I-A^b to biotin-binding sites. Saturation of the streptavidin conjugate was verified by nonreducing SDS-PAGE without boiling samples.

I-A^b α-chain. The extracellular domain of the I-A^b α-chain (underlined) was fused at its N-terminus to a secretion signal sequence (boundary denoted by "/") and at its C-terminus to an acidic leucine zipper and a recognition sequence for the BirA biotin ligase. MPCSRALILGVLALTTMLSLCGG/EDDIEADHVGTYGISVYQSPGDIGQYTFEFDGDELFYVDLDKKETVWMLPEFGQLASFDPQGGLQNIAVVKHNLGVLTKRSNSTPATNEAPQATVFPKSPVLLGQPNTLICFVDNIFPPVINITWLRNSKSVADGVYETSFFVNRDYSFHKLSYLTFIPSDDDIYDCKVEHWGLEEPVLKHWEPEIPAPMSELTETGGGGSTTAPSAQLEKELQALEKENAQLEWELQALEKELAQGGSGGSGLNDIFEAQKIEWHE.

I-A^b β-chain with $Tcaf3_{646–658}$(648Y) peptide (C4). The extracellular domain of the I-A^b β-chain (underlined) was fused at its N-terminus to a secretion signal sequence (boundary denoted by "/"), the $Tcaf3_{646–658}$(648Y) peptide (in bold), and a linker sequence and at its C-terminus to a basic leucine zipper and a 6xHis tag.

MALQIPSLLLSAAVVVLMVLSSPGTEG/**THYKAPWGELATD**GGGGTSGGGSGGSERHFVYQFMGECYFTNGTQRIRYVTRYIYNREEYVRYDSDVGEHRAVTELGRPDAEYWNSQPEILERTRAELDTVCRHNYEGPETHTSLRRLEQPNVVISLSRTEALNHHNTLVCSVTDFYPAKIKVRWFRNGQEETVGVSSTQLIRNGDWTFQVLVMLEMTPRRGEVYTCHVEHPSLKSPITVEWRAQSESAWSKGGGGSTTAPSAQLKKKLQALKKKNAQLKWKLQALKKKLAQHHHHHH.

I-A^b β-chain with $Tcaf3_{88-107}$ peptide (F1). The extracellular domain of the I-A^b β-chain (underlined) was fused at its N-terminus to a secretion signal sequence (boundary denoted by "/"), the $Tcaf3_{88-107}$ peptide (in bold), and a linker sequence and at its C-terminus to a basic leucine zipper and a 6xHis tag.

MALQIPSLLLSAAVVVLMVLSSPGTEG/**CPGAPIAVHSSLASLVNILG**GGGGTSGGGSGGSERHFVYQFMGECYFTNGTQRIRYVTRYIYNREEYVRYDSDVGEHRAVTELGRPDAEYWNSQPEILERTRAELDTVCRHNYEGPETHTSLRRLEQPNVVISLSRTEALNHHNTLVCSVTDFYPAKIKVRWFRNGQEETVGVSSTQLIRNGDWTFQVLVMLEMTPRRGEVYTCHVEHPSLKSPITVEWRAQSESAWSKGGGGSTTAPSAQLKKKLQALKKKNAQLKWKLQALKKKLAQHHHHHH.

I-A^b tetramer staining and enrichment

Tetramer staining was adapted from Tungatt et al. (2015). Cells were treated with dasatinib (AdooQ Bioscience) at a final

concentration of 50 nM for 30 min at 37°C in minimal staining buffer (PBS with 0.1% NaN_3, 2% normal rat serum, and 2% normal mouse serum, all from Jackson ImmunoResearch, and 10 µg/ml 2.4G2 antibody). PE- or allophycocyanin-labeled tetramers were added directly to dasatinib-treated cells in minimal staining buffer (without washing) at a final concentration of 100 nM for 1 h at room temperature. Cells were washed and incubated with unconjugated mouse anti-PE antibody (clone PE001; BioLegend) and mouse anti-allophycocyanin antibody (clone APC003; BioLegend) at a concentration of 10 µg/ml for 20 min at 4°C in minimal staining buffer. In some experiments (Figs. 4 and 5), tetramer-binding cells were not stained with unconjugated anti-PE and anti-allophycocyanin antibody but were instead enriched via one of two methods, which were adapted from Legoux and Moon (2012). In Fig. 4, A–C, cells were incubated with anti-PE and anti-allophycocyanin microbeads (Miltenyi Biotec) for 15 min on ice per the manufacturer's protocol, washed, and enriched over an autoMACS magnetic column. In Fig. 4, D–H; and Fig. 5, cells were treated with EasySep™ PE/APC Positive Selection Kits (STEMCELL Technologies) per the manufacturer's protocol with slight modification and enriched using a column-free magnet. The resulting bound fraction was stained and analyzed by flow cytometry as described below. The total number of tetramer$^+$ events was calculated as described by Legoux and Moon (2012).

Prostate tissue histology and immunohistology

Prostates were isolated as described below and fixed in 10% buffered formalin solution (Sigma) for 24–36 h. Paraffin-embedded, 5-µm-thick prostate sections were stained with H&E for blinded histopathology interpretation. Inflammation was graded from 0 to 4 (0 = none, 1 = very focal, 4 = extremely severe with loss of glandular section; scores 2 and 3 were increments between 1 and 4). For immunoperoxidase staining of mouse T cells, adjacent 5-µm-thick prostate sections were deparaffinized and hydrated. Endogenous peroxidase was blocked by Peroxidase Alkaline Phosphatase Blocking Reagent (Dako) and incubated overnight at 4°C with hamster anti-mouse CD3 monoclonal antibody (145-2C11; eBioscience) followed by goat anti-hamster IgG (1:100; Vector Laboratories) at room temperature. Samples were subsequently incubated with avidin-biotin complex (Vector Laboratories), and peroxidase was detected by 3,3′diaminobenzidine tetrahydrochloride (Vector Laboratories) until optimal color intensity was achieved. Counterstain was methylene blue.

Intrathymic injection of thymocytes

4×10^6 bulk thymocytes from MJ23tg$^+$ *Rag1*$^{-/-}$ CD45$^{.1/.1}$ females in 25 µl were injected intrathymically into 4–6-wk-old recipient mice and analyzed 7 d after transfer. Donor thymocytes were Foxp3$^-$ due to intraclonal competition in MJ23tg$^+$ *Rag1*$^{-/-}$ CD45$^{.1/.1}$ mice (Malchow et al., 2013). For analysis of CD4 SP thymocytes, 95% of whole thymus was depleted of CD8α$^+$ cells to enrich for CD4 SP thymocytes via column-free magnetic separation using biotin-conjugated anti-CD8α (53-6.7) and mouse streptavidin beads (STEMCELL Technologies) per the manufacturer's protocol.

CFA immunization

Mice were given a single subcutaneous injection in the flank of 100 µg peptide in 100 µl CFA emulsion (Sigma-Aldrich). CFA emulsion consisted of a 1:1 ratio peptide:CFA. Mice were analyzed 14 d later.

Generation of low-frequency MJ23tg chimeric mice

Bone marrow cells from MJ23tg$^+$ *Rag1*$^{-/-}$ CD45$^{.1/.1}$ and B6 females were T cell depleted in parallel via CD90.2 MACS MicroBeads (Miltenyi Biotec). A mixture consisting of 5% MJ23tg bone marrow and 95% B6 filler bone marrow was prepared, and 5×10^6 cells were retro-orbitally injected into sublethally (500 rads) irradiated host mice. Mice were analyzed at 6–8 wk after engraftment. For analysis of CD4 SP thymocytes, 95% of whole thymus was depleted of CD8α$^+$ cells to enrich for CD4 SP thymocytes via column-free magnetic separation using biotin-conjugated anti-CD8α (53-6.7) and mouse streptavidin beads (STEMCELL Technologies) per the manufacturer's protocol.

Generation of *Bim*$^{+/+}$/*Bim*$^{-/-}$ mixed BMC mice

Bone marrow cells from *Bim*$^{-/-}$ CD45$^{.2/.2}$ and B6.SJL CD45$^{.1/.1}$ males were isolated and enumerated. A mixture consisting of 50% *Bim*$^{-/-}$ CD45$^{.2/.2}$ and 50% B6.SJL CD45$^{.1/.1}$ was prepared, and 5×10^6 cells were retro-orbitally injected into lethally (900 rads) irradiated male B6.SJL CD45$^{.1/.1}$ host mice. 5–8 wk after engraftment, mice were immunized with 100 µg C4 peptide emulsified 1:1 in CFA.

Cell isolation and flow cytometry

Cells from SLOs were isolated into a single-cell suspension in RPMI 1640 medium supplemented with 10% FBS and 1× pen/strep (R10) using a 70-µm filter. Thymocytes were isolated in R10 using a 100-µm filter. To harvest prostatic lymphocytes, prostates were isolated from the genitourinary tract via microdissection, injected, and digested with Liberase TL (10 mg/ml; Roche) and DNase (20 mg/ml; Roche) in RPMI 1640 medium for 30 min at 37°C. Digested tissue was mechanically disrupted with frosted microscope slides, and viable lymphocytes were enriched using Histopaque 1119 (Sigma). All antibodies used were from BioLegend, eBioscience, or BD Biosciences. Cells were stained with conjugated antibodies specific for the following proteins (with clone name in parentheses): CD4 (GK1.5), CD8α (53–6.7), CD8β (Ly-3), CD3 (17A2), CD45.1 (A20), CD45.2 (104), CD69 (H1.2F3), Foxp3 (FJK-16s), B220 (RA3-6B2), CD11b (M1/70), CD11c (N418), F4/80 (BM8), anti-Thy1.1 (OX-7), anti-V_β3 TCR (KJ25), anti–PD-1 (RMP1-30), anti-CD44 (IM7), anti-TCRβ (H57-597), and anti–cleaved Caspase-3 (C92-605 RUO). Cells were stained for 20 min at 4°C in staining buffer (PBS with 2% FCS, 0.1% NaN_3, 5% normal rat serum, 5% normal mouse serum, and 5% normal rabbit serum, with all sera from Jackson ImmunoResearch, and 10 µg/ml 2.4G2 antibody). In experiments involving tetramer staining, cells were instead stained for 20 min at 4°C in minimal staining buffer (described above). Intracellular staining for Foxp3 and cleaved Caspase-3 was performed using fixation and permeabilization buffers (eBioscience). Flow cytometry was performed on an LSRFortessa (BD Biosciences), and data were analyzed using FlowJo v10.1 software (Tree Star).

TCR gene usage and CDR3 sequences

The MJ23 TCR contains the α-chain TRAV14-LYYNQGKLI, using TRAJ23, and the β-chain TRBV26-ASSLGSSYEQY, using TRBJ2-7. The SP33 TCR contains the α-chain TRAV9D-ALSMSVNYQLI, using TRAJ33, and the β-chain TRBV26-ASSLGSSYEQY, using TRBJ2-7.

Image acquisition

H&E and anti-CD3 immunohistochemistry slides were prepared as described above and examined with an Olympus BH2 light microscope with a 10× or 20× objective and with a 10× eyepiece, and were photographed with Lumenera's INFINITY 1-5 camera with Image Sensor Micron MT9P031 connected to an Apple computer. No postimage processing of color or contrast was performed.

Statistical analysis

Data were analyzed using Prism 8.1.2 (GraphPad Software). Significance testing was performed using the nonparametric Mann-Whitney test (two-tailed) or the Student *t* test (two-tailed), as specified in the figure legends. In Figs. 3 H and S2 H, a line of best fit was calculated using a log(x,y) transformation of the data, and linear regression analysis was performed using the extra-sum-of-squares F test (for y-intercept and slope parameters). No statistical methods were used to predetermine sample size.

Online supplemental material

Fig. S1 depicts C4/I-A^b and F1/I-A^b tetramer staining of $CD4^+$ T cells isolated from the prostates of *Aire*$^{-/-}$ mice, C4/I-A^b tetramer staining of immunized *Tcrb*$^{-/-}$ host mice reconstituted with *Tcaf3(C4)*$^+$ or *Tcaf3(C4)*$^{-/-}$ $CD4^+$ T cells as in Fig. 2, and representative histology and C4/I-A^b tetramer staining of the prostates of *Tcrb*$^{-/-}$ host mice as in Fig. 2. Fig. S2 depicts analysis of *Tcaf3(C4)*$^+$ and *Tcaf3(C4)*$^{-/-}$ low-frequency MJ23tg chimeric mice for hallmarks of antigen experience and clonal deletion as in Fig. 3. Fig. S3 depicts Helios expression by C4/I-A^b tetramer$^+$ cells after immunization of *Tcaf3(C4)*$^+$ male mice and analysis of *Tcrb*$^{-/-}$ mice reconstituted with congenically distinct T reg and T conv cells.

Acknowledgments

We thank Dengping Yin and the University of Chicago Microsurgery Core Facility for their assistance with intrathymic injections. We thank the University of Chicago Cytometry and Antibody Technologies Facility for their assistance and troubleshooting. We thank the University of Chicago Human Tissue Resource Center for processing of fixed tissue samples.

This work was funded by National Institutes of Health grant R01-AI126756 (to E.J. Adams and P.A. Savage). D.E.J. Klawon, D.C. Gilmore, J.L. Chao, M.T. Walker, and R.K. Duncombe were supported by National Institutes of Health grant T32-AI007090. J.D. Leonard was a Robert Black Fellow of the Damon Runyon Cancer Research Foundation (DRG-2251-16). C.H. Miller was supported by a National Cancer Institute predoctoral fellowship (F30-CA236061) and by the University of Chicago Medical Scientist Training Program (T32-GM007281).

Author contributions: D.E.J. Klawon contributed to the study design, performed experiments, interpreted data, and wrote the manuscript; D.C. Gilmore contributed to the study design, performed experiments, and interpreted data; J.D. Leonard, C.H. Miller, J.L. Chao, and M.T. Walker performed experiments; J.D. Leonard and R.K. Duncombe designed and generated recombinant protein and tetramer reagents; K.S. Tung performed image acquisition and analysis of tissue pathology; E.J. Adams contributed to the study design and data interpretation; and P.A. Savage designed the study, interpreted data, and wrote the manuscript. All authors contributed to the discussion.

Disclosures: D.C. Gilmore reported grants from National Institute of Cancer and grants from National Institute of Allergy and Infectious Disease during the conduct of the study and personal fees from Compass Therapeutics and personal fees from TCR2 Therapeutics outside the submitted work. J.D. Leonard reported personal fees from 3T Biosciences outside the submitted work. No other disclosures were reported.

Submitted: 13 April 2020
Revised: 17 December 2020
Accepted: 29 March 2021

References

Bautista, J.L., C.W. Lio, S.K. Lathrop, K. Forbush, Y. Liang, J. Luo, A.Y. Rudensky, and C.S. Hsieh. 2009. Intraclonal competition limits the fate determination of regulatory T cells in the thymus. *Nat. Immunol.* 10: 610–617. https://doi.org/10.1038/ni.1739

Bouillet, P., J.F. Purton, D.I. Godfrey, L.C. Zhang, L. Coultas, H. Puthalakath, M. Pellegrini, S. Cory, J.M. Adams, and A. Strasser. 2002. BH3-only Bcl-2 family member Bim is required for apoptosis of autoreactive thymocytes. *Nature.* 415:922–926. https://doi.org/10.1038/415922a

Breed, E.R., M. Watanabe, and K.A. Hogquist. 2019. Measuring Thymic Clonal Deletion at the Population Level. *J. Immunol.* 202(11):3226–3233. https://doi.org/10.4049/jimmunol.1900191

Crawford, F., H. Kozono, J. White, P. Marrack, and J. Kappler. 1998. Detection of antigen-specific T cells with multivalent soluble class II MHC covalent peptide complexes. *Immunity.* 8:675–682. https://doi.org/10.1016/S1074-7613(00)80572-5

DeVoss, J., Y. Hou, K. Johannes, W. Lu, G.I. Liou, J. Rinn, H. Chang, R.R. Caspi, L. Fong, and M.S. Anderson. 2006. Spontaneous autoimmunity prevented by thymic expression of a single self-antigen. *J. Exp. Med.* 203: 2727–2735. https://doi.org/10.1084/jem.20061864

Fan, Y., W.A. Rudert, M. Grupillo, J. He, G. Sisino, and M. Trucco. 2009. Thymus-specific deletion of insulin induces autoimmune diabetes. *EMBO J.* 28:2812–2824. https://doi.org/10.1038/emboj.2009.212

Fujimoto, N., Y. Akimoto, T. Suzuki, S. Kitamura, and S. Ohta. 2006. Identification of prostatic-secreted proteins in mice by mass spectrometric analysis and evaluation of lobe-specific and androgen-dependent mRNA expression. *J. Endocrinol.* 190:793–803. https://doi.org/10.1677/joe.1.06733

Hassler, T., E. Urmann, S. Teschner, C. Federle, T. Dileepan, K. Schober, M.K. Jenkins, D.H. Busch, M. Hinterberger, and L. Klein. 2019. Inventories of naive and tolerant mouse CD4 T cell repertoires reveal a hierarchy of deleted and diverted T cell receptors. *Proc. Natl. Acad. Sci. USA.* 116: 18537–18543. https://doi.org/10.1073/pnas.1907615116

Hogquist, K.A. 2001. Assays of thymic selection. Fetal thymus organ culture and in vitro thymocyte dulling assay. *Methods Mol. Biol.* 156:219–232.

Josefowicz, S.Z., L.F. Lu, and A.Y. Rudensky. 2012. Regulatory T cells: mechanisms of differentiation and function. *Annu. Rev. Immunol.* 30: 531–564. https://doi.org/10.1146/annurev.immunol.25.022106.141623

Klein, L., E.A. Robey, and C.S. Hsieh. 2019. Central $CD4^+$ T cell tolerance: deletion versus regulatory T cell differentiation. *Nat. Rev. Immunol.* 19: 7–18. https://doi.org/10.1038/s41577-018-0083-6

Lee, H.M., J.L. Bautista, J. Scott-Browne, J.F. Mohan, and C.S. Hsieh. 2012. A broad range of self-reactivity drives thymic regulatory T cell selection to limit responses to self. *Immunity*. 37:475–486. https://doi.org/10.1016/j.immuni.2012.07.009

Legoux, F.P., and J.J. Moon. 2012. Peptide:MHC tetramer-based enrichment of epitope-specific T cells. *J. Vis. Exp.* (68):4420. https://doi.org/10.3791/4420

Leonard, J.D., D.C. Gilmore, T. Dileepan, W.I. Nawrocka, J.L. Chao, M.H. Schoenbach, M.K. Jenkins, E.J. Adams, and P.A. Savage. 2017. Identification of natural regulatory T cell epitopes reveals convergence on a dominant autoantigen. *Immunity*. 47:107–117.e8. https://doi.org/10.1016/j.immuni.2017.06.015

Leung, M.W., S. Shen, and J.J. Lafaille. 2009. TCR-dependent differentiation of thymic Foxp3+ cells is limited to small clonal sizes. *J. Exp. Med.* 206:2121–2130. https://doi.org/10.1084/jem.20091033

Malchow, S., D.S. Leventhal, S. Nishi, B.I. Fischer, L. Shen, G.P. Paner, A.S. Amit, C. Kang, J.E. Geddes, J.P. Allison, et al. 2013. Aire-dependent thymic development of tumor-associated regulatory T cells. *Science*. 339:1219–1224. https://doi.org/10.1126/science.1233913

Malchow, S., D.S. Leventhal, V. Lee, S. Nishi, N.D. Socci, and P.A. Savage. 2016. Aire enforces immune tolerance by directing autoreactive T cells into the regulatory T cell lineage. *Immunity*. 44:1102–1113. https://doi.org/10.1016/j.immuni.2016.02.009

Malhotra, D., J.L. Linehan, T. Dileepan, Y.J. Lee, W.E. Purtha, J.V. Lu, R.W. Nelson, B.T. Fife, H.T. Orr, M.S. Anderson, et al. 2016. Tolerance is established in polyclonal CD4(+) T cells by distinct mechanisms, according to self-peptide expression patterns. *Nat. Immunol.* 17:187–195. https://doi.org/10.1038/ni.3327

McDonald, B.D., J.J. Bunker, S.A. Erickson, M. Oh-Hora, and A. Bendelac. 2015. Crossreactive αβ T cell receptors are the predominant targets of thymocyte negative selection. *Immunity*. 43:859–869. https://doi.org/10.1016/j.immuni.2015.09.009

Meng, J., E.A. Mostaghel, F. Vakar-Lopez, B. Montgomery, L. True, and P.S. Nelson. 2011. Testosterone regulates tight junction proteins and influences prostatic autoimmune responses. *Horm. Cancer*. 2:145–156. https://doi.org/10.1007/s12672-010-0063-1

Moon, J.J., H.H. Chu, M. Pepper, S.J. McSorley, S.C. Jameson, R.M. Kedl, and M.K. Jenkins. 2007. Naive CD4(+) T cell frequency varies for different epitopes and predicts repertoire diversity and response magnitude. *Immunity*. 27:203–213. https://doi.org/10.1016/j.immuni.2007.07.007

Moon, J.J., H.H. Chu, J. Hataye, A.J. Pagán, M. Pepper, J.B. McLachlan, T. Zell, and M.K. Jenkins. 2009. Tracking epitope-specific T cells. *Nat. Protoc.* 4:565–581. https://doi.org/10.1038/nprot.2009.9

Morita, S., T. Kojima, and T. Kitamura. 2000. Plat-E: an efficient and stable system for transient packaging of retroviruses. *Gene Ther.* 7:1063–1066. https://doi.org/10.1038/sj.gt.3301206

Nelson, R.W., D. Beisang, N.J. Tubo, T. Dileepan, D.L. Wiesner, K. Nielsen, M. Wüthrich, B.S. Klein, D.I. Kotov, J.A. Spanier, et al. 2015. T cell receptor cross-reactivity between similar foreign and self peptides influences naive cell population size and autoimmunity. *Immunity*. 42:95–107. https://doi.org/10.1016/j.immuni.2014.12.022

Samy, E.T., L.A. Parker, C.P. Sharp, and K.S. Tung. 2005. Continuous control of autoimmune disease by antigen-dependent polyclonal CD4+CD25+ regulatory T cells in the regional lymph node. *J. Exp. Med.* 202:771–781. https://doi.org/10.1084/jem.20041033

Savage, P.A., J.J. Boniface, and M.M. Davis. 1999. A kinetic basis for T cell receptor repertoire selection during an immune response. *Immunity*. 10:485–492. https://doi.org/10.1016/S1074-7613(00)80048-5

Setiady, Y.Y., K. Ohno, E.T. Samy, H. Bagavant, H. Qiao, C. Sharp, J.X. She, and K.S. Tung. 2006. Physiologic self antigens rapidly capacitate autoimmune disease-specific polyclonal CD4+ CD25+ regulatory T cells. *Blood*. 107:1056–1062. https://doi.org/10.1182/blood-2005-08-3088

Shevach, E.M. 2009. Mechanisms of foxp3+ T regulatory cell-mediated suppression. *Immunity*. 30:636–645. https://doi.org/10.1016/j.immuni.2009.04.010

Taniguchi, R.T., J.J. DeVoss, J.J. Moon, J. Sidney, A. Sette, M.K. Jenkins, and M.S. Anderson. 2012. Detection of an autoreactive T-cell population within the polyclonal repertoire that undergoes distinct autoimmune regulator (Aire)-mediated selection. *Proc. Natl. Acad. Sci. USA*. 109:7847–7852. https://doi.org/10.1073/pnas.1120607109

Thébault-Baumont, K., D. Dubois-Laforgue, P. Krief, J.P. Briand, P. Halbout, K. Vallon-Geoffroy, J. Morin, V. Laloux, A. Lehuen, J.C. Carel, et al. 2003. Acceleration of type 1 diabetes mellitus in proinsulin 2-deficient NOD mice. *J. Clin. Invest.* 111:851–857. https://doi.org/10.1172/JCI16584

Thornton, A.M., P.E. Korty, D.Q. Tran, E.A. Wohlfert, P.E. Murray, Y. Belkaid, and E.M. Shevach. 2010. Expression of Helios, an Ikaros transcription factor family member, differentiates thymic-derived from peripherally induced Foxp3+ T regulatory cells. *J. Immunol.* 184:3433–3441. https://doi.org/10.4049/jimmunol.0904028

Tungatt, K., V. Bianchi, M.D. Crowther, W.E. Powell, A.J. Schauenburg, A. Trimby, M. Donia, J.J. Miles, C.J. Holland, D.K. Cole, et al. 2015. Antibody stabilization of peptide-MHC multimers reveals functional T cells bearing extremely low-affinity TCRs. *J. Immunol.* 194:463–474. https://doi.org/10.4049/jimmunol.1401785

Turner, V.M., S. Gardam, and R. Brink. 2010. Lineage-specific transgene expression in hematopoietic cells using a Cre-regulated retroviral vector. *J. Immunol. Methods*. 360:162–166. https://doi.org/10.1016/j.jim.2010.06.007

Yang, S., N. Fujikado, D. Kolodin, C. Benoist, and D. Mathis. 2015. Immune tolerance. Regulatory T cells generated early in life play a distinct role in maintaining self-tolerance. *Science*. 348:589–594. https://doi.org/10.1126/science.aaa7017

Supplemental material

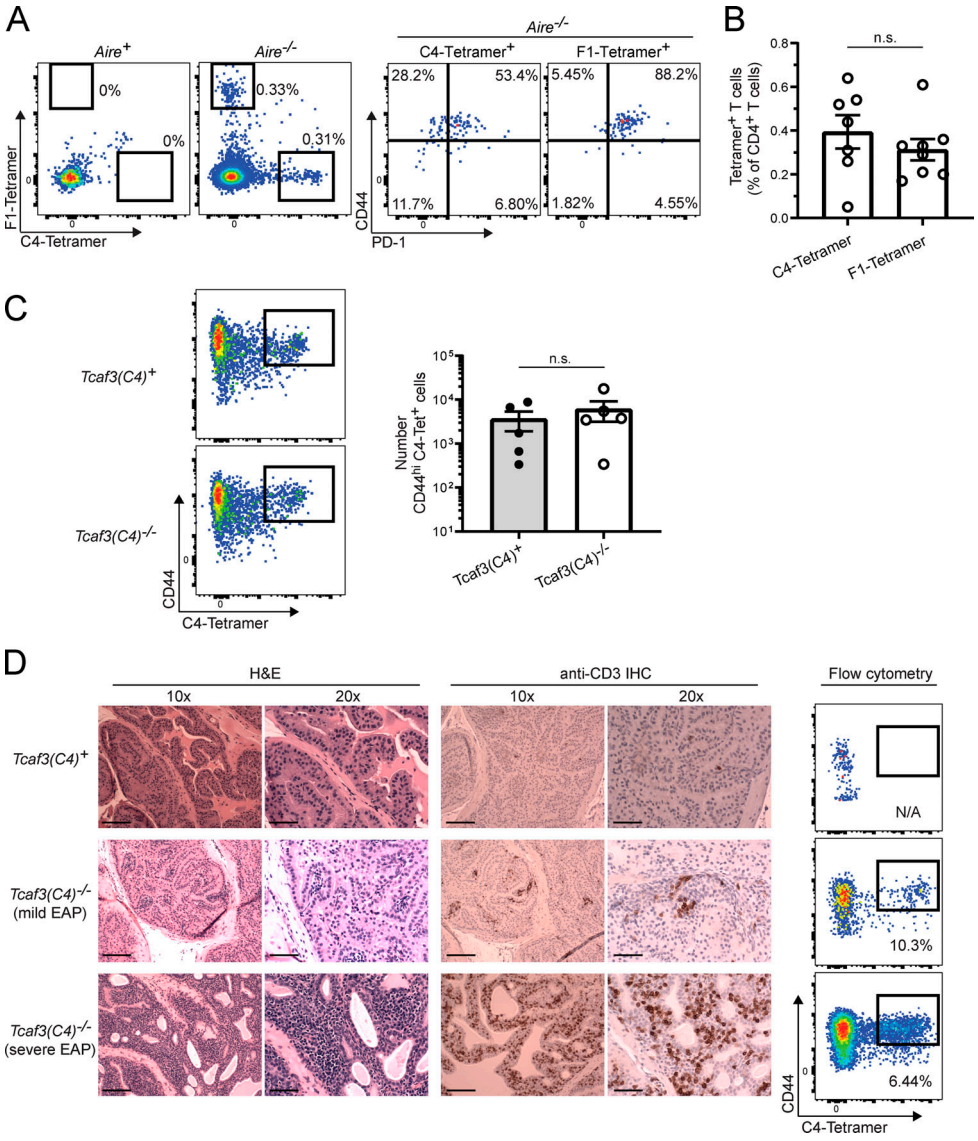

Figure S1. **Following T cell transfer, C4/I-A^b-specific T cells are detectable in recipient mice and can induce mild or severe prostatitis when not previously selected on C4/I-A^b. (A and B)** Both C4/I-A^b and F1/I-A^b are antigenic and recurrently targeted by CD4$^+$ T cells in settings of Aire deficiency. Lymphocytes were enriched from the prostates of >15-wk-old *Aire*$^+$ or *Aire*$^{-/-}$ male littermate mice and analyzed by flow cytometry for C4/I-A^b tetramer- and F1/I-A^b tetramer-binding cells. **(A)** Representative flow cytometric analysis of CD4$^+$ T cells isolated from the prostates of mice of the indicated genotype. The left plots depict C4/I-A^b tetramer-allophycocyanin vs. F1/I-A^b tetramer-PE staining of polyclonal CD4$^+$ T cells, whereas the right plots depict PD-1 vs. CD44 expression by tetramer$^+$ T cells. The frequency of cells within the indicated gates is denoted. Data are representative of two independent experiments. **(B)** Summary plot of the pooled data from A (left) showing the frequency of C4/I-A^b tetramer$^+$ and F1/I-A^b tetramer$^+$ cells among polyclonal CD4$^+$ T cells isolated from the prostates of *Aire*$^{-/-}$ mice. Each symbol represents one mouse. n = 7, C4; n = 8, F1. Mean ± SEM is indicated (n.s., P > 0.05; two-tailed Mann-Whitney test). Data are pooled from two independent experiments. **(C)** Following T cell transfer, C4/I-A^b–specific T cells are detectable in recipient mice following peptide immunization. 10^7 polyclonal CD4$^+$ T cells were isolated from the pooled SLOs of 8–12-wk-old *Tcaf3(C4)*$^+$ or *Tcaf3(C4)*$^{-/-}$ male donors and transferred intravenously into *Tcrb*$^{-/-}$ *Tcaf3(C4)*$^{+/+}$ male littermate recipients. 3 wk after transfer, host mice were immunized subcutaneously with 100 µg C4 peptide emulsified in CFA. 14 d after immunization, CD4$^+$ T cells were isolated from the pooled SLOs and analyzed by flow cytometry. Left: Representative flow cytometric analysis depicting CD44 vs. C4/I-A^b tetramer expression by polyclonal CD4$^+$ T cells isolated from the pooled SLOs of recipient *Tcrb*$^{-/-}$ males of the indicated genotype. Right: Summary plot of pooled data showing the absolute number of CD44^{hi} C4/I-A^b tetramer$^+$ CD4$^+$ T cells isolated from the pooled SLOs of recipient *Tcrb*$^{-/-}$ males of the indicated genotype. Each symbol represents one mouse. n = 5, *Tcaf3(C4)*$^+$; n = 5, *Tcaf3(C4)*$^{-/-}$. Mean ± SEM is indicated (n.s., P > 0.05; two-tailed Mann-Whitney test). Data are representative or pooled from three independent experiments. **(D)** T cell–deficient mice reconstituted with CD4$^+$ T cells from *Tcaf3(C4)*$^{-/-}$ donors can develop mild or severe prostatitis. 10^7 polyclonal CD4$^+$ T cells were isolated from the pooled SLOs of 8–12-wk-old *Tcaf3(C4)*$^+$ or *Tcaf3(C4)*$^{-/-}$ male donors and transferred i.v. into *Tcrb*$^{-/-}$ *Tcaf3(C4)*$^{+/+}$ male littermate recipients. 9 wk after transfer, lobes from one side of the prostate were taken for tissue pathology, while lobes from the contralateral side were analyzed by flow cytometry. Representative H&E images (left), anti-CD3 immunohistochemistry (IHC) images (middle), and flow cytometric analysis depicting CD44 vs. C4/I-A^b tetramer expression by polyclonal CD4$^+$ T cells (right) of the prostates from host mice. The image magnification (left and middle) and frequency of cells within the indicated gates (right) are denoted; scale bars = 100 µm at 10× and 50 µm at 20×. Of six recipient mice that received CD4$^+$ donor cells from *Tcaf3(C4)*$^{-/-}$ males and were subjected to histological analysis, two presented with experimental autoimmune prostatitis (EAP), and three contained CD3$^+$ cell clusters in the prostate. Zero of five mice that received CD4$^+$ cells from *Tcaf3(C4)*$^+$ donors developed EAP or contained CD3$^+$ cell clusters in the prostate. N/A, not applicable.

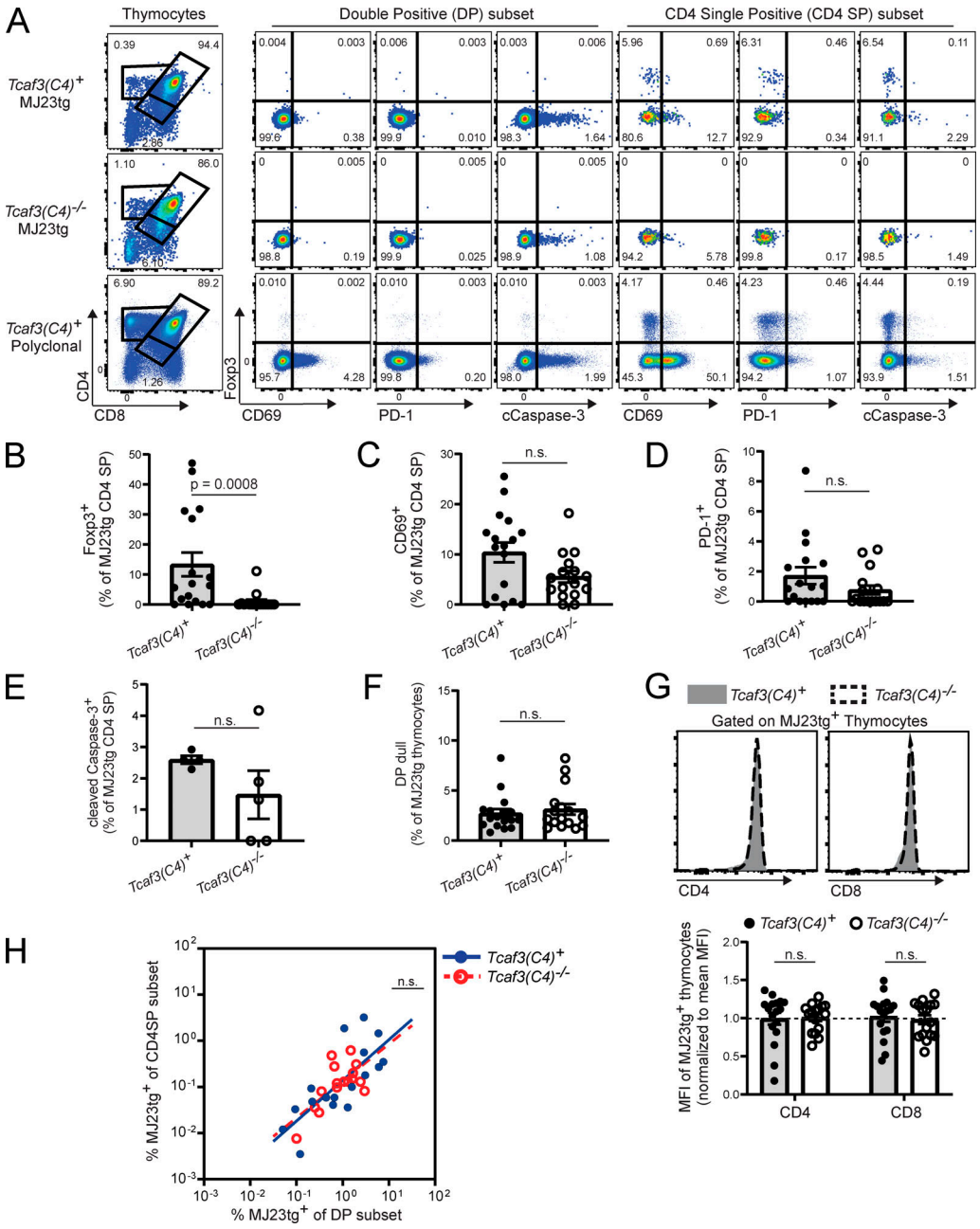

Figure S2. **In the thymus of low-frequency MJ23tg BMCs, C4/I-A^b–dependent clonal deletion does not impact monoclonal MJ23tg thymocytes (related to Fig. 3).** Low-frequency MJ23tg BMCs were generated by reconstitution of sublethally irradiated 4–6-wk-old *Tcaf3(C4)*$^+$ or *Tcaf3(C4)*$^{-/-}$ CD45$^{.2/.2}$ littermate males with a mix of 95% wild-type B6 bone marrow + 5% MJ23tg *Rag1*$^{-/-}$ CD45$^{.1/.1}$ bone marrow (see Materials and methods). Mice were analyzed 6 wk after BMC generation. **(A)** Representative flow cytometric analysis of MJ23tg (top and middle rows) or polyclonal (bottom row) thymocytes isolated from *Tcaf3(C4)*$^+$ and *Tcaf3(C4)*$^{-/-}$ host mice. The leftmost plots depict CD4 vs. CD8 expression by indicated CD45$^+$ thymocytes, while the remaining plots depict Foxp3, CD69, PD-1, and cleaved Caspase-3 (cCaspase-3) expression by CD4$^+$CD8$^+$ DP and CD4 SP thymocytes. The frequency of cells within the indicated gates is denoted. Data are representative of at least two independent experiments. **(B–F)** Summary plots of pooled data from A showing the frequency of MJ23tg CD4 SP thymocytes expressing Foxp3 (B), CD69 (C), PD-1 (D), cCaspase-3 (E), and CD4^{dull} CD8^{dull} (DP dull; F) isolated from the indicated host mice. Each symbol represents one mouse. n = 17, *Tcaf3(C4)*$^+$; n = 16, *Tcaf3(C4)*$^{-/-}$ (B–D). n = 4, *Tcaf3(C4)*$^+$; n = 5, *Tcaf3(C4)*$^{-/-}$ (E). n = 17, *Tcaf3(C4)*$^+$; n = 16, *Tcaf3(C4)*$^{-/-}$ (F). Mean ± SEM is indicated (n.s., P > 0.05; two-tailed nonparametric Mann-Whitney test). Data are pooled from multiple independent experiments: three (B–D), two (E), and three (F). **(G)** Top: Representative flow cytometric analysis of CD4 and CD8 expression by MJ23tg thymocytes isolated from the indicated host mice. Bottom: Summary plots of pooled data showing the MFI of CD4 and CD8 by MJ23tg thymocytes isolated from the indicated host mice, normalized to the mean MFI of all MJ23tg thymocytes in each independent experiment. The average MFI of each independent experiment was normalized to 1, indicated by the dashed line. Each symbol represents one mouse. n = 17, *Tcaf3(C4)*$^+$; n = 16, *Tcaf3(C4)*$^{-/-}$. Mean ± SEM is indicated (n.s., P > 0.05; two-tailed nonparametric Mann-Whitney test). Data are representative or pooled from three independent experiments. **(H)** Scatter plot depicting the frequency of MJ23tg thymocytes among polyclonal CD4 SP thymocytes vs. the frequency of MJ23tg thymocytes among polyclonal DP thymocytes. Each symbol represents one mouse. n = 17, *Tcaf3(C4)*$^+$; n = 16, *Tcaf3(C4)*$^{-/-}$. Line indicates best-fit curve using linear regression analysis (extra-sum-of-squares F test). Data are pooled from three independent experiments.

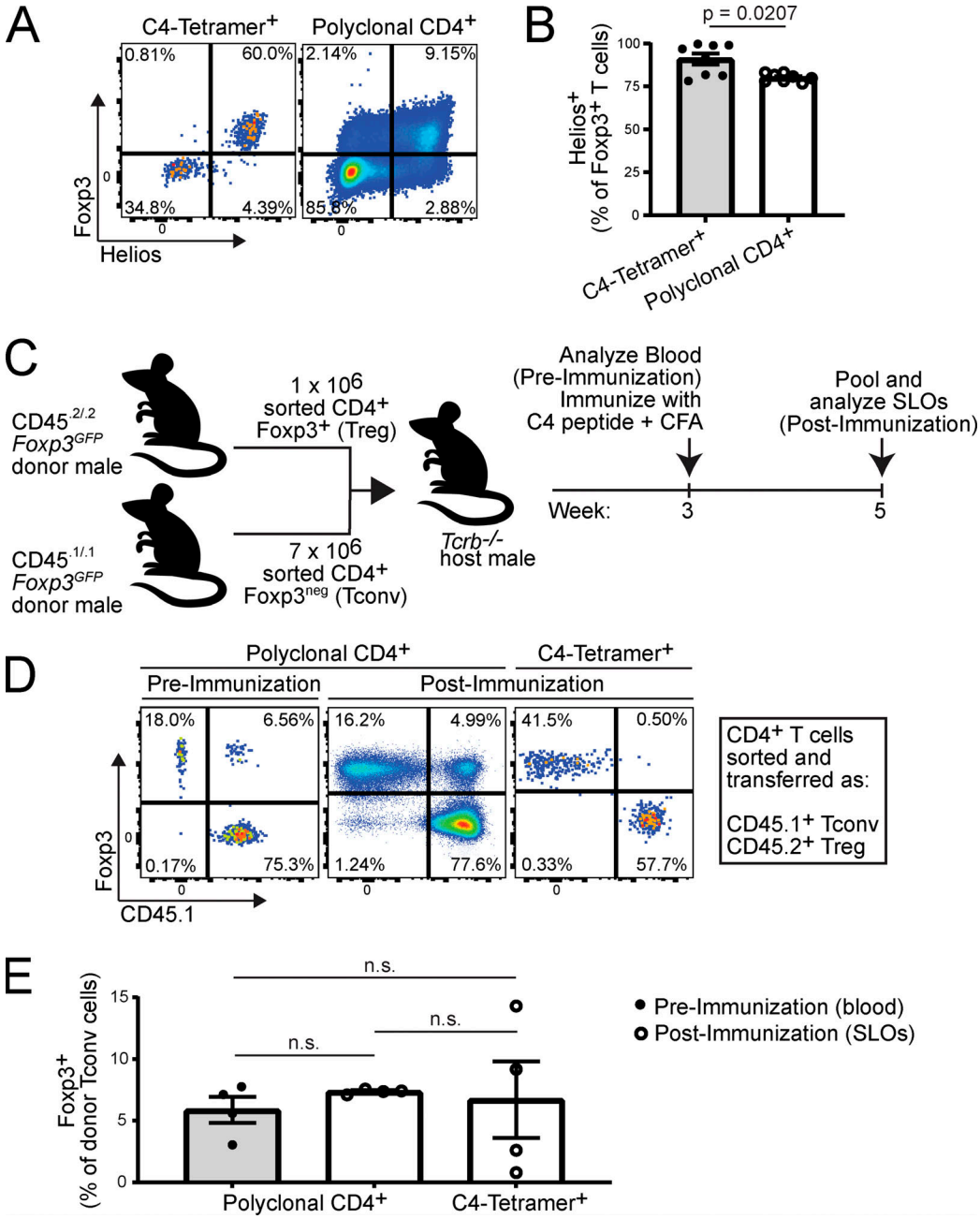

Figure S3. **C4 peptide immunization does not induce the peripheral differentiation of C4-specific T reg cells from T conv cells. (A and B)** 4–6-wk-old naive *Tcaf3(C4)*$^{+}$ or *Tcaf3(C4)*$^{-/-}$ male and female littermate mice were immunized subcutaneously with 100 µg C4 peptide emulsified in CFA. 14 d after immunization, CD4^{+} T cells were isolated, and C4/I-A^{b} tetramer-binding cells were enriched from the pooled SLOs and analyzed by flow cytometry. **(A)** Representative flow cytometric analysis of CD4^{+} T cells enriched from the pooled SLOs of mice of the indicated genotype depicting Foxp3 vs. Helios expression by double C4/I-A^{b} tetramer^{+} CD4^{+} T cells (left) and polyclonal CD4^{+} T cells (right). The frequency of cells within the indicated gates is denoted. Data are representative of two independent experiments. **(B)** Summary plot of data pooled from A showing the frequency of double C4/I-A^{b} tetramer^{+} CD4^{+} Foxp3^{+} T reg cells or polyclonal CD4^{+} Foxp3^{+} T reg cells expressing Helios enriched from the pooled SLOs from mice of the indicated genotype. Each symbol represents one mouse (n = 8). Mean ± SEM is indicated (two-tailed nonparametric Mann-Whitney test). Data are pooled from two independent experiments. **(C)** Experimental schematic for D and E. 10^{6} Foxp3^{+} CD45.2^{+} and 7 × 10^{6} Foxp3^{-} CD4^{+} CD45.1^{+} T cells were sorted from congenically disparate *Foxp3*^{GFP} male donors and cotransferred into *Tcrb*$^{-/-}$ male littermate recipients. 3 wk after transfer, blood was collected and analyzed by flow cytometry, and mice were immunized subcutaneously with 100 µg C4 peptide emulsified in CFA. 14 d after immunization, CD4^{+} T cells were isolated from the pooled SLOs of recipient mice, stained with C4/I-A^{b} tetramer, and analyzed by flow cytometry. **(D)** Representative flow cytometric analysis depicting CD45.1 vs. Foxp3 expression by CD4^{+} T cells isolated from host mice. The left plot depicts polyclonal CD4^{+} T cells isolated from the blood preimmunization, the middle plot depicts polyclonal CD4^{+} T cells isolated from the pooled SLOs after immunization, and the right plot depicts double C4/I-A^{b} tetramer^{+} CD4^{+} T cells isolated from the pooled SLOs after immunization. The frequency of cells within the indicated gates is denoted. Data are representative of two independent experiments. **(E)** Summary plot of pooled data from D showing the frequency of Foxp3^{+} cells among congenically marked CD4^{+} T cells that were initially transferred as Foxp3^{-} T conv cells. Each symbol represents one mouse (n = 4). Mean ± SEM is indicated (n.s., P > 0.05; two-tailed nonparametric Mann-Whitney test). Data are pooled from two independent experiments.